NAVAL POSTGRADUATE SCHOOL
Monterey, California

THESIS

DEVELOPMENT OF A 1/7-SCALE F/A-18 UAV FOR SUPERMANEUVERABILITY RESEARCH

by

Michael S. Shelton

September 1991

Thesis Advisor: Richard M. Howard

Approved for public release; distribution is unlimited.

Unclassified

Security Classification of this page

REPORT DOCUMENTATION PAGE

1a Report Security Classification: Unclassified
1b Restrictive Markings
2a Security Classification Authority
3 Distribution Availability of Report: Approved for public release; distribution is unlimited.
2b Declassification/Downgrading Schedule
4 Performing Organization Report Number(s)
5 Monitoring Organization Report Number(s)
6a Name of Performing Organization: Naval Postgraduate School
6b Office Symbol (If Applicable): AA
7a Name of Monitoring Organization: Naval Postgraduate School
6c Address (city, state, and ZIP code): Monterey, CA 93943-5000
7b Address (city, state, and ZIP code): Monterey, CA 93943-5000
8a Name of Funding/Sponsoring Organization
8b Office Symbol (If Applicable)
9 Procurement Instrument Identification Number
8c Address (city, state, and ZIP code)
10 Source of Funding Numbers

Program Element Number	Project No	Task No	Work Unit Accession No

11 Title (Include Security Classification): DEVELOPMENT OF A 1/7TH SCALE F/A-18 UAV FOR SUPERMANEUVERABILITY RESEARCH

12 Personal Author(s): Shelton, Michael S.

13a Type of Report	13b Time Covered	14 Date of Report (year, month,day)	15 Page Count
Master's Thesis	From 10-1-90 To 9-26-91	September 1991	128

16 Supplementary Notation: The views expressed in this thesis are those of the author and do not reflect the official policy or position of the Department of Defense or the U.S. Government.

17 Cosati Codes			18 Subject Terms (continue on reverse if necessary and identify by block number)
Field	Group	Subgroup	UAV, Supermaneuverability, Forebody strakes, Leading Edge Extension (LEX)

19 Abstract (continue on reverse if necessary and identify by block number

A 1/7-scale F/A-18 Hornet UAV was constructed for use in generic fighter high-angle-of-attack research. The aircraft, purchased as a kit, has been extensively modified to incorporate rudders and trailing edge flaps. In addition, an emergency parachute recovery system (EPRS) was installed for use in the event of departure from controlled flight, loss of radio signal, structural failure or any other anomally that would preclude a normal landing recovery. Parachute performance data and design considerations are discussed. Aerodynamic and dynamic data have been determined, such as cg, moments of inertia, full and empty weights, surface areas, aspect ratio and wing loading. Preliminary performance estimations have been determined and the aircraft has been flown. Future research to include the employment of non-conventional yaw control methods using forebody strakes and possibly pneumatic blowing is discussed. The need to pursue cooperative thesis research in the investigation of a Digital Flight Control System (DFCS), utilizing fly-by-wire active flight controls, is discussed. This UAV generic fighter program is planned as a multi-thesis student project, and this thesis documents the research and work of the second student involved with the project.

20 Distribution/Availability of Abstract
[X] unclassified/unlimited [ ] same as report [ ] DTIC users

21 Abstract Security Classification: Unclassified

22a Name of Responsible Individual: Richard M. Howard
22b Telephone (Include Area code): (408) 646-2870
22c Office Symbol: AAHo

DD FORM 1473, 84 MAR 83 APR edition may be used until exhausted
All other editions are obsolete

security classification of this page: Unclassified

Approved for public release; distribution is unlimited.

"DEVELOPMENT OF A 1/7- SCALE F/A-18 UAV FOR SUPERMANEUVERABILITY RESEARCH"

by

Michael S. Shelton
Lieutenant Commander, United States Navy
B. of AE., Auburn University, 1977

Submitted in partial fulfillment of the requirements
for the degree of

MASTER OF SCIENCE IN AERONAUTICAL ENGINEERING

from the

NAVAL POSTGRADUATE SCHOOL
September 1991

ABSTRACT

A 1/7-scale F/A-18 Hornet UAV was constructed for use in generic fighter high-angle-of-attack research. The aircraft, purchased as a kit, has been extensively modified to incorporate rudders and trailing edge flaps. In addition, an emergency parachute recovery system (EPRS) was installed for use in the event of departure from controlled flight, loss of radio signal, structural failure or any other anomally that would preclude a normal landing recovery. Parachute performance data and design considerations are discussed. Aerodynamic and dynamic data have been determined, such as cg, moments of inertia, full and empty weights, surface areas, aspect ratio and wing loading. Preliminary performance estimations have been determined and the aircraft has been flown. Future research to include the employment of non-conventional yaw control methods using forebody strakes and possibly pneumatic blowing is discussed. The need to pursue cooperative thesis research in the investigation of a Digital Flight Control System (DFCS), utilizing fly-by-wire active flight controls, is discussed. This UAV generic fighter program is planned as a multi-thesis student project, and this thesis documents the research and work of the second student involved with the project.

TABLE OF CONTENTS

LIST OF TABLES

LIST OF FIGURES

LIST OF SYMBOLS AND ABBREVIATIONS

AAM	Air-to-Air Missile
ACM	Air Combat Maneuvering
AIM	"Air Intercept Missile" designation, such as AIM-7M Sparrow
AOA	Angle of attack
AR	Aspect ratio, b^2/S
BHP	Brake horsepower
BVR	Beyond Visual Range
C_D	Three-dimensional drag coefficient
C_{D_i}	Induced drag coefficient, $C_L^2/\pi eAR$
C_{D_0}	Zero-lift drag coefficient of an aircraft; characteristic total drag coefficient of parachute or other decelerator device
C_{l_β}	Rolling moment coefficient due to sideslip
$C_{l_{\delta_a}}$	Rolling moment coefficient due to aileron deflection
C_L	Three-dimensional lift coefficient
C_{L_α}	$dC_L/d\alpha$, slope of C_L vs α
C_{M_α}	Slope of the moment coefficient curve, $dC_M/d\alpha$
$C_{M_{ac}}$	Three-dimensional pitching moment about the aerodynamic center
$C_{M_{cg}}$	Total pitching moment about the center of gravity

$C_{M_{\delta_e}}$	Pitching moment coefficient due to elevator deflection
C_{M_o}	Pitching moment coefficient at zero angle of attack
C_{M_q}	Pitching moment coefficient due to pitch rate
C_{n_β}	Yawing moment coefficient with a change in sideslip β
$C_{n_{\delta_r}}$	Yawing moment coefficient due to rudder deflection
$C_{n_{strake}}$	Yawing moment coefficient due to deployment of forebody strake
C_R	Wingroot chord length
C_T	Wingtip chord length
C_{y_β}	Side force coefficient due to sideslip
D_C	Parachute constructed diameter
D_0	Parachute reference diameter based on its reference area. In the case of flat circular canopies, D_C is the same as D_0.
EPRS	Emergency parachute recovery system
FBW	Fly-by-wire
FCS	Flight control system
HP	Horsepower
ID	Identification, as in "positive ID"
I_{xx}	Moment of Inertia about the longitudinal (roll) axis
I_{yy}	Moment of Inertia about the lateral (pitch) axis

I_{zz}	Moment of Inertia about the vertical (yaw) axis
I_{xz}	Product of inertia about the xz axis
KCAS	Knots calibrated airspeed
KIAS	Knots indicated airspeed
KTAS	Knots true airspeed
LE	Leading edge
LED	Leading edge down
LEU	Leading edge up
NASA	National Aeronautics and Space Administration
OOC	Out of control flight
Q	Dynamic pressure, = $1/2\rho v^2$, also q
R_e	Reynolds number, $R_e = \rho vc/\mu$
RIO	Radar Intercept Officer
ROD	Rate of descent
RPV	Remotely piloted vehicle
SAM	Surface-to-air missile
S_{ht}	Horizontal tail area
S_{LEX}	Leading edge extension area
S_0	Parachute reference area. Always its uninflated planform area.
S_w	Wing area

S_{vt}	Vertical tail area
TE	Trailing edge
TED	Trailing edge down
TEL	Trailing edge left
TER	Trailing edge right
TEU	Trailing edge up
THP	Thrust horsepower
TOPGUN	Slang for Navy Fighter Weapons School (NFWS)
UAV	Unmanned aerial vehicle
V_F	Vertical tail volume
V_H	Horizontal tail volume

a_o	Lift curve slope of a 2-D airfoil
a_t	Lift-curve slope of horizontal tail
a_w	Lift-curve slope of wing
ac	Aerodynamic center
b	Wing span
c	Wing chord
$\bar{c}$	Mean aerodynamic chord, m.a.c.
cg	Center of gravity, also c.g. or CG

d	Forebody reference diameter
e	Oswald efficiency factor
g	Acceleration due to gravity, 32.174 ft/sec^2; also G
h	Location of cg in percent m.a.c.
h_{ac}	Location of aerodynamic center in percent m.a.c.
h_n	Stick-fixed neutral point in percent m.a.c.
h_n'	Stick-free neutral point in percent m.a.c.
$\bar{l}$	Reference distance between jack points/landing gear weight for cg determination (Equations 2 and 3)
l	Distance between wing and horizontal tail quarter chords
l_F	Vertical tail length
l_l	Parachute suspension line length
l_t	Horizontal tail length
m.a.c.	Mean aerodynamic chord, $\bar{c}$
n	Load factor, the number of g's acceleration
p	Roll rate
q	Pitch rate
r	Yaw rate
q	Dynamic pressure, = $1/2\rho v^2$, also Q
v	Freestream velocity

x_{cg}	Distance forward of a reference point for cg determination
$\overline{y}$	Distance outward from the aircraft fuselage centerline to the m.a.c.
α	Angle of attack
β	Angle of sideslip
Λ	Wingsweep angle
λ	Taper ratio, C_T/C_R; model scaling factor
μ	Dynamic viscosity
ρ	Air density, slug/ft^3

ACKNOWLEDGMENTS

It is imperative that one who successfully completes an arduous undertaking be reflective and thankful upon those who provided so much guidance and comfort during both the lighter and darker periods of the work. First, I wish to thank my God and Creator for the ability and privilege to pursue graduate education, without Whom nothing would matter, and for His presence when things became seemingly insurmountable.

To my wife and family, from whom most of the motivation to work hard and to attempt great achievements came, so that we can have a better life in the future. I thank them very much for their patience and long-suffering sacrifice during this long journey called Naval Postgraduate School. Thank you Ann, Michael and Heather.

Great and many thanks to my thesis advisor Professor Rick Howard for his guidance and direction of this project. He has a tremendous vision for UAV research that certainly needs more funding and brighter students than me. A special, sincere thank you to Professor Ed Wu for allowing me the after-hours use of his office and facilities. Additionally, many thanks to Don Meeks of the the NPS Aeronautics and Astronautics Department UAV Lab for his design and construction assistance and insight, and to Mike Callaway for his extensive volunteer time and invaluable ducted-fan model experience to lend assistance in the form of equipment, engine break-in, thrust testing and tuning as the airplane was made ready for flight.

And many thanks also to Mr. Richard White of NASA Langley in Hampton, Virginia, who contributed invaluable documentation, advice and insight in the final preparation phases before the first flight of the aircraft.

I. INTRODUCTION

Most of the basic philosophy for what makes a good fighter aircraft did not significantly change from the days of WWI until after WWII. Things were simple: get behind your opponent, close until you could see the fabric patches or wing rivets, and open fire. However, the advent of the jet aircraft introduced the notion that the role of dogfighting in Air Combat Maneuvering (ACM) just might be over. The Korean conflict momentarily brought the dogfight back into vogue, with close-in aerial combat between F-86 Sabres and MiG-15's involving the only weapon still at hand: the air-to-air gun employed by a skillful gunner. But after Korea, rapid advances in air-to-air missile technology with the creation of the now famous (and long-lived) AIM-9 Sidewinder, and soon after the AIM-4 Falcon and the AIM-7 Sparrow radar guided air-to-air missiles (AAM's), along with increasingly faster and heavier jet fighters, seemed to seal forever the bygone days of the classic dogfight [Ref. 1]. Envisioned were future engagements that would employ the long range missile shot, hopefully deploying one's air-to-air missile prior to the enemy's release of his, and thus gaining the kill: guns would no longer be needed. Soon, as the 1950's were drawing to a close, the long range engagement in the Beyond Visual Range (BVR) scenario was being touted as the future of air combat.

A. THE DOGFIGHT QUESTION

The modern fighter pilot is still faced with the decision whether to engage in ACM with his opponent. The engagement decision will be the result of a

complex set of rules and doctrine, and of course, tempered with judgement, much training, and the flow of adrenaline. Normally, it can be said that the dogfight is the result of a poor intercept. One would ideally like to see his opponent(s) blow up a few miles in front of the windscreen, with all "bogeys" accounted for. Although ACM is the focus of extensive training, and is the most fun and exciting of all the fighter missions, in reality it is the most dangerous arena of air combat tactics, and should be avoided in real air warfare. The participating aircraft decay rapidly to very slow speeds (energy states), making them predictable and easy prey for the "wild card" joining the fight from outside the "furball". Fuel consumption increases dramatically, since each participant will almost always be using maximum thrust. For example, the F-14 and F-15, in maximum afterburner, have fuel flow rates of about 2000 lbs/min (300 gal/min). Thus, if unavoidable, the fight must be enjoined and consummated with either a quick kill of the opponent(s) or a quick decision to disengage. In either case, an egress from the fight must be made immediately. It is well known in the fighter community that the ACM arena demands superior weapons, maneuverability, agility and longitudinal acceleration.

The Vietnam War was a rude awakening for air combat tactics [Ref.1]. Almost overnight, the United States discovered that its aircraft were ill equipped to perform the close encounters of ACM, for the requirements for BVR shots were often greatly restricted with the need to positively identify (ID) the target. Careless missile engagements could and did result in "Blue-on-Blue" engagements, needlessly shooting down aircraft on our side. On the other hand, we soon discovered that too often the targets being intercepted were real bandits, but identification was too late to employ a radar missile (AIM-7), being inside

the Sparrow's minimum range. Worse, the heavy, poor-turning F-4's were confronted with enemy aircraft with superior turning ability and agility, able to easily turn inside the lumbering Phantom's turn radius. Additionally, the MiG-15, -17 and -21 also had guns. The F-4 had no internal gun until the F-4E came along in the late 60's, and was the only variant produced with an internal gun. Additionally, the F-4E had an improved radar (the APQ-120) and extended leading edge slats that automatically deployed at high angles of attack, providing about 33 percent more lift [Ref.1], thus improving controllability and stability in the ACM arena. But combat tactics were very poor for both the Air Force and the Navy. The early days of the Vietnam War were filled with stories of surprised pilots, Phantom pilots included, trying to escape a barrage of tracers over the canopy, and too often the end result was a kill for an aggressive North Vietnamese pilot if he chose to press the fight. During one engagement against three MiG-17's, the war's first Aces, LT Randy Cunningham and LTJG Willie Driscoll, his Radar Intercept Officer (RIO) occupying the rear seat, pulled 12 G's in a high-G barrel-roll-underneath, a last-ditch maneuver to try to escape their gunfire. Only their F-4's incredible strength and superior acceleration, along with opportune cloud cover, allowed them to escape and return to the ship. After landing, their Phantom was a write-off because of major structural damage from the severe, 12-G overstress, and had to be pushed over the side after salvage of usable equipment. Later, on 10 May 1972, on the very flight where LT Cunningham and LTJG Driscoll gained their 3rd, 4th and 5th kills, LT Cunningham downed North Vietnam's leading pilot (13 air-to-air kills), Colonel Tomb, in a fight he had no right to win: F-4J vs MiG-17. Only tenacity, superb skill using the vertical, and mistakes by his opponent allowed Cunningham and

Driscoll to down Colonel Tomb with an AIM-9 Sidewinder as the experienced North Vietnamese pilot attempted a desperate disengagement from the fight. As it was, LT Cunningham and LTJG Driscoll were also critically low on fuel from the prolonged fight, and were downed by an SA-2 surface-to-air missile (SAM) as they attempted to nurse the Phantom on fumes toward an airborne tanker off the North Vietnamese coast. They were shot down from flying at max endurance speed to save fuel, and were thus a predictable and easy target. Therefore, it was a one-for-one exchange of fighter assets [Ref. 1].

A combination of having non-agile aircraft, an awkward weapons suite, poor ID procedures, and virtually no corporate memory left in the dogfight arena at first proved deadly for the United States (prior to 1970). Even with the U.S. Navy's F-8 Crusader as our best dogfighter, employing four 20-mm cannons and four AIM-9 Sidewinder heat seeking missiles, it still often proved little match for a well-flown, aggressively-piloted MiG-17 or MiG-21.

Out of this dire situation was born the Navy Fighter Weapons School in 1968, later to become a squadron in its own right, and better known today as TOPGUN. The tactics and aggressive flying taught at TOPGUN provided the pivotal turning point in the Navy's air combat scene. In 1968, Air Force and Navy fighter crews had about a 2-to-1 kill ratio against the North Vietnamese air force. By 1972, however, when the air campaign began again in earnest in the north, the kill ratio quickly jumped to 12-to-1, almost exclusively because of the training that TOPGUN and similar Air Force programs provided.

B. MODERN AND FUTURE FIGHTER AGILITY REQUIREMENTS

The survivability and effectiveness of today's and tomorrow's fighters depend on many complex factors, not the least of which is how to deal with the

post-stall flight regime. Since close-in ACM is still inevitable in future air combat, new aircraft must be designed and extensively evaluated in the high-angle-of-attack regime. After the engagement has deteriorated to the "knife fight in the phone booth" stage, the opponent with the best maneuverability and agility will have the advantage. The importance of being able to maintain directional control, maintain smooth pitch authority, and point the nose to bring a weapon to bear cannot be overemphasized in a dogfight [Ref. 2]. Control effectiveness is key.

C. CURRENT HIGH AOA DIRECTIONAL CONTROL INVESTIGATIONS

There has been much research in recent years dealing specifically with the directional control problem at high angles of attack [Ref. 2, 3, 4 and 5], and the subsequent development of non-conventional control methods to counter the yaw instability. All conventional fighters exhibit decreasing yaw stability as the angle of attack increases, with the parallel problem of decreasing rudder effectiveness to initiate yaw rates or roll due to yaw, or simply to maintain directional control in dynamic maneuvering (Figure 1). Loss of control eventually occurs if the angle of attack becomes too great, and any perturbation that induces angular motion in the yaw axis usually causes departure from controlled flight, which may result in loss of the aircraft. The main two areas of specific interest for the tactical jet in the high-AOA regimes are Post Stall and Deep Stall. Post Stall is that area of high AOA flight where the aircraft is no longer producing useful lift, but may still be controllable in pitch, roll and yaw. Deep Stall is concerned with high AOA flight where the aircraft is unable to reduce the angle of attack

by normal inputs to flight controls. This is just one phase of out-of-control flight. It requires use of an anti-spin chute or other similar device for recovery.

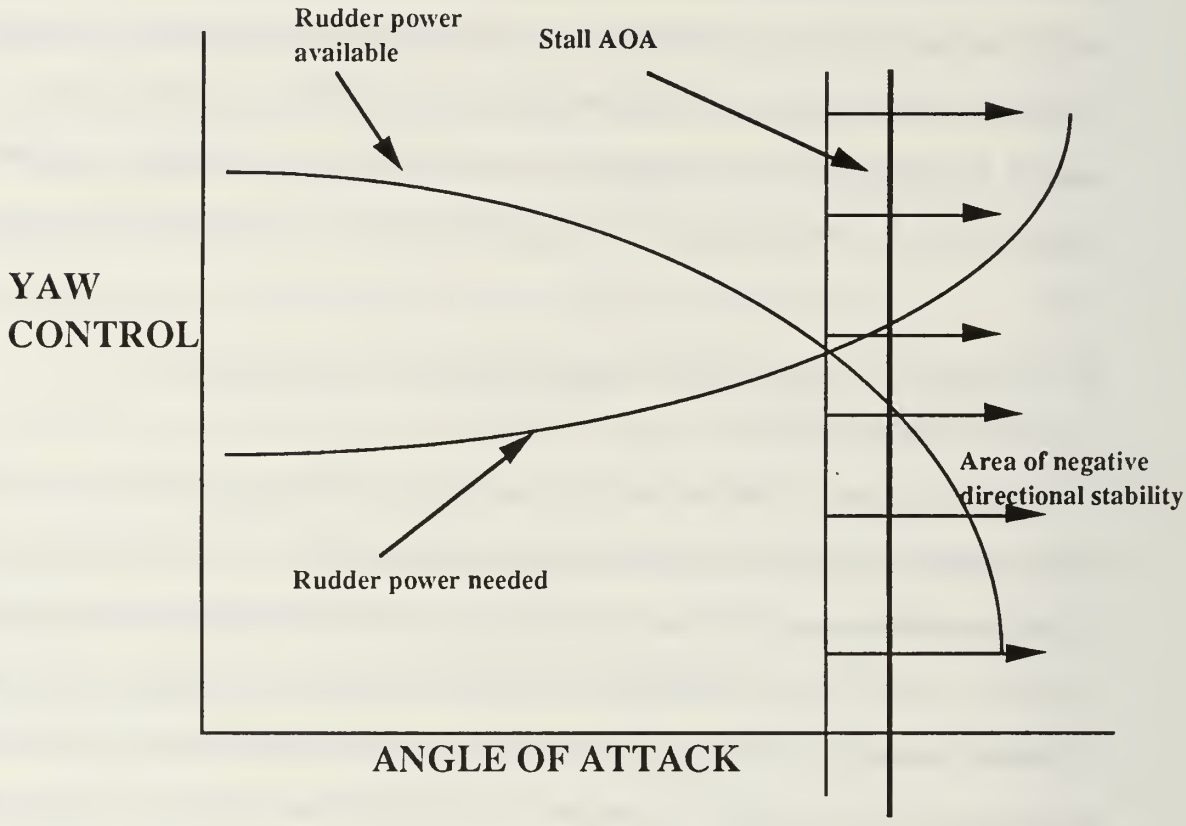

Figure 1 Generic yawing moment versus angle of attack.

Current research includes a full-scale effort with an F/A-18 Hornet in NASA Ames' largest (80'X120') wind tunnel [Ref. 6 and 7], which is a follow-on program to the wind and water tunnel research of References 2 through 5. Specifically, investigations are centered around the use of controllable strakes at

or near the front of the radome on the forebody of the F/A-18 to control or manipulate the vortex shedding process at high angles of attack, and thus induce desired yawing moments. The use of pneumatic methods in the form of tangentially blowing air along the forebody near the nose has also been extensively studied, and will be investigated in the full-scale F/A-18 of Reference 7, but so far pneumatic methods with scale models have shown less promise than the use of strakes.

D. ROLE OF THE UAV IN HIGH AOA AND FIGHTER AGILITY RESEARCH

A generic fighter UAV, scaled and instrumented appropriately, can carry on the research beyond the wind tunnel and into free flight where both quantitative and qualitative analyses can be directly observed. A research fighter UAV carries decreased risks in systems and in human costs, and is much more inexpensive than a full-scale effort. In essence, the UAV effort efficiently bridges the gap between the wind-tunnel testing and the full-scale efforts, reducing time and money necessary to conduct investigations of the post-stall regime. The next chapter reviews a variety of UAV programs, which include both pure research and reconnaissance vehicles, and both dynamically and non-dynamically-scaled types, including fighter and other tactical models. Chapter IV will include discussion of current fighter/tactical aircraft scale-model programs germane to the current research with the F/A-18 UAV.

II. CURRENT UAV/RPV PROGRAMS

A discussion is in order for a few selected U.S. and International UAV/RPV research and military programs.

A. UNITED STATES PROGRAMS

1. NASA

a. Dynamically-Scaled Drop Models

NASA is extensively involved with model and UAV testing at the Langley Research Center in Hampton, Virginia. Much of this research involves testing of dynamically-scaled models, in both a vertical-flow wind tunnel and in free-flight, whereby the model is radio controlled with pre-planned flight control configurations in the deep-stall regime, dealing with maneuverability, departure and spin recovery techniques [Ref. 6, 8 and 9]. A few of the drop-model testing examples include: F-4, F-14, F-15, B-1, F/A-18, F-16XL, X-29A, and X-31.

Drop-model tests are performed by releasing the dynamically-scaled models from a specially-configured helicopter at 6000 feet AGL. These models are normally about 1/5th scale, about eight to ten feet long, with a weight of approximately 300 pounds. After release, the model pilot on the ground performs the prescribed test maneuvers and flight control configurations until 1500 feet AGL. The test is then concluded, the model is recovered, if able, into normal flight, glided toward a desirable recovery zone, and the recovery parachute deployed for the final descent phase [Ref. 9]. The models are not powered.

b. Exdrone RPV Flight Tests

The United States Marines, through the Naval Air Test Center at Naval Air Station Patuxent River, requested the NASA Langley Research Center to conduct flight test investigations for the Exdrone (Expendable Drone) RPV to improve the handling characteristics, especially at slow speeds [Ref. 10]. The tests were conducted at NASA Langley's Plum Tree Test Site, and resulted in much improved flight characteristics, including the elimination of the severe wing rock problem as the aircraft approached stall prior to landing [Ref. 11]. The Exdrone is described later in more detail.

c. Spin Resistant Dynamically-Scaled Trainer

A cooperative research effort with a private aviation firm was conducted with a generic, 1/4th scale, single-engine, pusher-propeller configuration basic trainer to determine the spin and controllability characteristics involved with a drooped outer leading edge [Ref. 12]. In both this case and that of the Exdrone research, the models were conventionally flown in the takeoff and landing modes, with no parachute or other unusual recovery systems employed.

d. Helicopters

NASA Langley has an active scale-model helicopter program researching such disciplines as rotor blade acoustics and efficiencies. They are also developing a suitable autopilot for the largest scale-model helicopter they have, the "Bruiser", a 1/5th scale model made by Pacific RPV. Additionally, cameras are placed in strategic areas on the helicopters for detailed recording of blade dynamics.

2. Army

Except for the Aquila program, the Army has fewer demands for UAV programs than the Navy and Marines. Much testing has been conducted with the Aquila, which was the subject of a large-scale parachute recovery test program in the mid 1980's by Lockheed Missiles and Space Company [Ref. 13], the prime contractor for the program. However, the Army does have the Pioneer aircraft and deployed a Pioneer System (about five aircraft) during Operation Desert Storm, using them mainly as reconnaissance systems for their Apache helicopters. The Army is also in need of a Battalion Targeting System (BTS) UAV system, but Army Laboratory Command plans to award study contracts were cancelled because of burdensome contracting problems [Ref. 14:pp. 32-33].

3. Navy and Marine Corps

Both services used UAV's to a great extent in Operations Desert Shield and Desert Storm. The Navy found the Pioneer UAV system invaluable for battleship gunnery corrections, providing unprecedented accuracy and efficiency of the many rounds fired [Ref. 15]. The Marines also used the Pioneer for artillery spotting and troop reconnaissance. Additionally, the Exdrone was extensively used by the Marines to look over the next hill for troop movements, location of enemy armor, etc. [Ref. 14, 15]. Navy and Marine Corps systems are described below.

a. The Pioneer UAV System

Encouraged by the Israeli use of the Mastiff UAV, then Secretary of the Navy John Lehman procured some Mastiffs for Marine use in a study which was enormously successful [Ref. 14]. With the completion of that study, a contract for an off-the-shelf UAV system called Pioneer, manufactured by the

AAI Corporation in Maryland, was awarded in 1985. It has a 17 foot wingspan, weighs about 420 pounds, has a cruise speed of 115 mph, and has about a four hour endurance. It is equipped with a variety of sensor payloads, including daytime cameras and nighttime low-light TV and infrared systems. The Pioneer enjoyed great success in Operation Desert Storm, flying 980 hours with the Marines, 641 hours with the Navy and 155 hours with the Army [Ref. 16]. Only one was confirmed downed by hostile fire. About a dozen more were lost because of mechanical failures (engine failure, loss of radios, etc.), and several were damaged but returned safely to home base. With artillery and naval guns, the Pioneer allowed very quick adjustment of aim points, sometimes causing the target to be destroyed in as little as only three rounds. In previous conflicts (Lebanon, Vietnam and WWII), as many as 50 rounds would be fired in a statistical pattern to safely assume the target had been likely destroyed [Ref. 14]. The UAV came into its own in Iraq and Kuwait, and proved invaluable to battlefield and naval commanders.

b. The Exdrone System

Several hundred BQM-147A Exdrone (Expendable Drone) UAV's were in stock before Desert Storm began, and about 60 were sent to the Marines. The Exdrone is a delta wing, tractor-propulsion configuration RPV with a ready-to-fly empty weight of 46 pounds and an approximate 34-pound payload [Refs. 10 and 11]. The aircraft is relatively inexpensive, costing less than $10,000 per copy, including the camera payload. Thus, the name EXpendable DRONE. Yet, it is normally recovered by landing on a runway, strip or road. With an eight-foot-span delta-planform flying wing, constructed primarily of wood, foam and fiberglass, the Exdrone has an extremely low radar cross section

(RCS). The Exdrone employs mostly off-the-shelf components, including a common, commercially-available flight control system, Sachs two-stroke chain saw engine of seven horsepower, and commercially-available color camcorder camera adapted for the airborne surveillance mission. The sensor package downlinks to a hand-held color TV unit carried inside a portable metal suitcase to the Marine user in the field [Ref. 10] for real-time reconnaissance. The Exdrone allowed the Marines to be able to move into southern Kuwait City a day and a half earlier than planned [Ref. 14].

c. The TALD (Tactical Air-Launched Decoy)

The TALD UAV is an unpowered decoy dual sourced by Israeli Military Industries (IMI) and Brunswick Corporation Defense Division that is carried by A-6E, F/A-18 and S-3 aircraft, with plans to include the F-16 in the future. No special modifications are required for carriage; it weighs 400 pounds and costs approximately $25,000. It is programmed before launch for one of any number of flight profiles that can simulate an attacking aircraft [Ref. 10]. The TALD proved quite successful in the opening hours and days of the air war against targets in Iraq and Kuwait, accounting for the waste of many Iraqi surface-to-air assets. Approximately 200 TALD's were launched in Operation Desert Storm. Most of the TALD performance data generated during Desert Storm is classified. Plans are proceeding for an Engineering Change Proposal (ECP) to modify the TALD into the Improved TALD (ITALD), which would be powered by a small Williams International jet engine [Ref. 14 and 17] to sustain higher speeds and allow a loitering capability.

d. Medium Range Unmanned Aerial Vehicle

The UAV Joint Project and Cruise Missile Project Offices are currently evaluating the feasibility of an advanced Medium Range UAV based on the BQM-145A aerial target airframe [Ref. 19]. The UAV-MR would be equipped with the Advanced Tactical Air Reconnaissance System (ATARS) for high resolution imagery in the visible and infrared spectrum. This payload is either a low altitude electro-optical or infrared line scanner imagery sensor package, along with appropriate data link equipment, capable of conducting conventional and contingency combat operations in situations including biological and chemical warfare conditions. Launch can be either by land, sea or air platforms, to include the F/A-18C/D and F-16. Recovery is by parachute, and the air vehicle can either touch down in the water or be retrieved in mid-air by helicopter. The flight envelope is expected to include altitudes of 100 to 40,000 feet and a maximum speed of 550 KTAS/.9 Mach.

B. INTERNATIONAL PROGRAMS

Current foreign programs that were highlighted because of Desert Storm are described below. More detailed descriptions of U.S and International UAV/RPV programs can be found in Reference 18.

1. Great Britain

British forward artillery positions used CL-89 drones for artillery spotting. The CL-89 is built by Bombardier Canadair [Ref. 14].

2. France

The French used the Apilles Mini Avion de Reconnaissance Telepilote (MART) drone for real-time, behind the enemy lines reconnaissance. During the war, this system was responsible for the discovery and subsequent destruction of

Iraqi supply points. It is built by a consortium of European companies and military agencies [Ref. 14].

C. NAVAL POSTGRADUATE SCHOOL UAV PROGRAMS

The UAV research program in the Department of Aeronautics and Astronautics has current projects investigating high AOA aerodynamics, aircraft performance and flying qualities, non-conventional vertical-flight stability, and rotorcraft vibration reduction using higher-harmonic control. Instrumentation needs to support the research projects include the measurement of control-surface deflections, angle of attack, sideslip angle, airspeed and throttle position. A seven-channel telemetry system has been developed for the downlink of this data to a receiving unit and flight recorder. Brief descriptions of the various air vehicles employed in the research efforts follow.

1. 1/2-Scale Pioneer UAV

This aircraft was procured for flight data to support Pioneer simulation efforts at the Pacific Missile Test Center (PMTC) and to identify potential solutions to problems encountered in fleet use of the full-scale Pioneer aircraft [Ref. 20]. Expected use also includes experience needed for the future operation of the large NASA Mini-Sniffer UAV on loan to the Aeronautics and Astronautics Department [Ref. 18].

2. ARCHYTAS Tilting-Ducted-Fan UAV

This UAV is unique, with a mostly conventional airframe with the horizontal tail and dual vertical stabilizers mounted on twin booms extending aft from the wings, but employing a shrouded propeller/fan unit at the center of gravity that can be tilted to align the propeller/fan exhaust rearward in the conventional manner, 90 degrees downward, or anywhere in between. A 1/2-

scale technology demonstrator has been designed and built and is undergoing testing. Investigations will center on V/STOL performance and stability, using movable vanes in the propeller/fan slipstream for yaw, pitch and roll control during hover and very slow speed flight. A current difficulty with this project is finding an engine and propeller/fan combination with sufficient thrust in the constrained duct area to achieve vertical flight for the 25-pound aircraft. Lessons learned will be applied to the full-scale vehicle design.

3. Remotely-Piloted Helicopters

The UAV helicopter program consists of two small-scale (about 1/8th), commercially-available models, the Legend, manufactured by GMP, and the Helistar, manufactured by Schluter. Additionally, the UAV Lab has a Bruiser, built by Pacific RPV, similar to the one in NASA Langley's program. The two smaller 1/8th helicopters are used mainly for proficiency and pilot training for the larger Bruiser, and are also being utilized to validate accelerometer and rate-gyro instrumentation for larger vehicles. The Bruiser is the subject of research in higher harmonic control of the main rotor blades for vibration reduction. Current work includes instrumenting the vehicle with vibration-sensing accelerometers and a telemetry package.

4. 1/8th Scale F-16 Falcon UAV

The F-16 is a commercially-available and quite popular Byron's Originals Aircraft R/C model with retractable gear, powered by a ducted-fan, two-stroke glow plug R/C engine (Figures 2 and 3). It weighs approximately 15 pounds, and is the current testbed for the aforementioned instrumentation and data telemetry recording and analysis system, from which the model's performance and stability derivatives may be determined. The F-16 has

demonstrated excellent flying qualities and has sufficient fuel for extended test sessions exceeding eight to ten minutes. It is the primary validation vehicle for the telemetry system scheduled for future use in the 1/2-scale Pioneer UAV and the F/A-18 UAV. There are no current plans to operate the F-16 at high AOA and in supermaneuverability/agility flight tests because of weight restrictions with the vehicle.

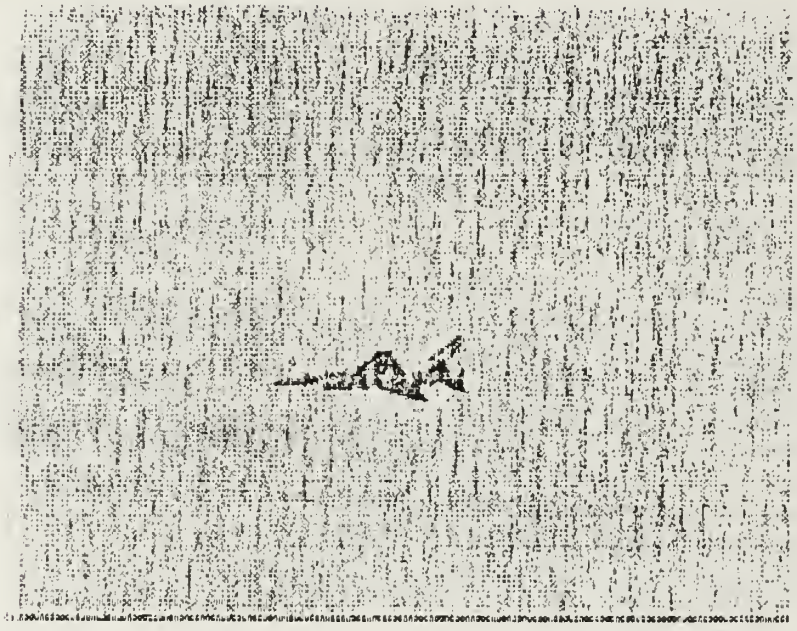

Figure 2 F-16 UAV during flight test.

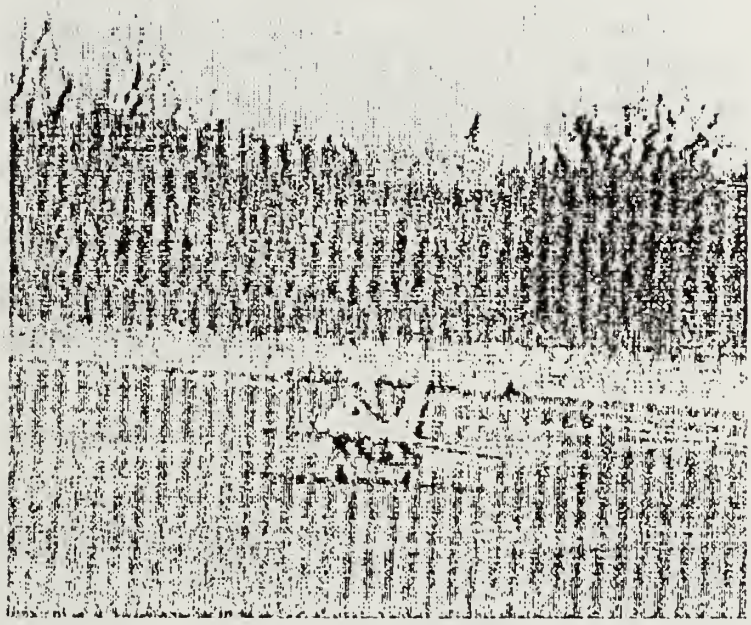

Figure 3 F-16 UAV landing.

5. 1/7th F/A-18 Hornet UAV

This UAV is the subject of this thesis, and was procured and built to test in the very high AOA regime to investigate non-conventional yaw control techniques as applied to a generic fighter aircraft.

III. 1/7-SCALE F/A-18 UAV DESIGN AND CONSTRUCTION

Work on the F/A-18 UAV commenced in October 1990, when the program was taken over from LT Dan Lee (of Reference 18). His focus included the initial procurement of the kit, initial construction and assembly of the necessary tooling, materials and support hardware. Additionally, he prudently decided an emergency parachute recovery system would be needed for safety of the UAV, and thus added those necessary materials and engineering expertise to the program.

The ultimate focus of this UAV program is low-speed aerodynamic research in the high-AOA flight, post-stall regime where non-conventional yaw control methods can be investigated, utilizing some or all of the forebody-strake techniques investigated in References 2 through 4, and possibly the pneumatic blowing methods of Reference 5. Once the F/A-18 UAV enters a flight test program with proper instrumentation, then aircraft stability and control derivatives can be determined and the final phases of supermaneuverability investigation can commence. Further examination of this future research is discussed in Chapter IV.

The reader will note the F/A-18 UAV is not accurately dynamically scaled in any parameter (structurally, stiffness, power, weight, moments of inertia, vibration response, endurance, and so forth), nor was it the intent to do so. Again, the goal is the investigation of several current non-conventional directional control methods that have been researched by a variety of sources. As the program continues to evolve, perhaps fly-by-wire flight controls can be

added to complement the high AOA research and provide another dimension for flight test. This will also be discussed in more detail in Chapter IV.

A. DESCRIPTION OF THE MODEL

The F/A-18 Hornet UAV is a single-seat replica, ducted-fan powered model kit with retractable landing gear, manufactured by the Yellow Aircraft Company of Puyallup, Washington (Figures 4 and 5). It has a fiberglass fuselage and canopy, with the wings, horizontal and vertical tails made of pre-shaped foam cores covered with thin balsa skin [Ref. 21].

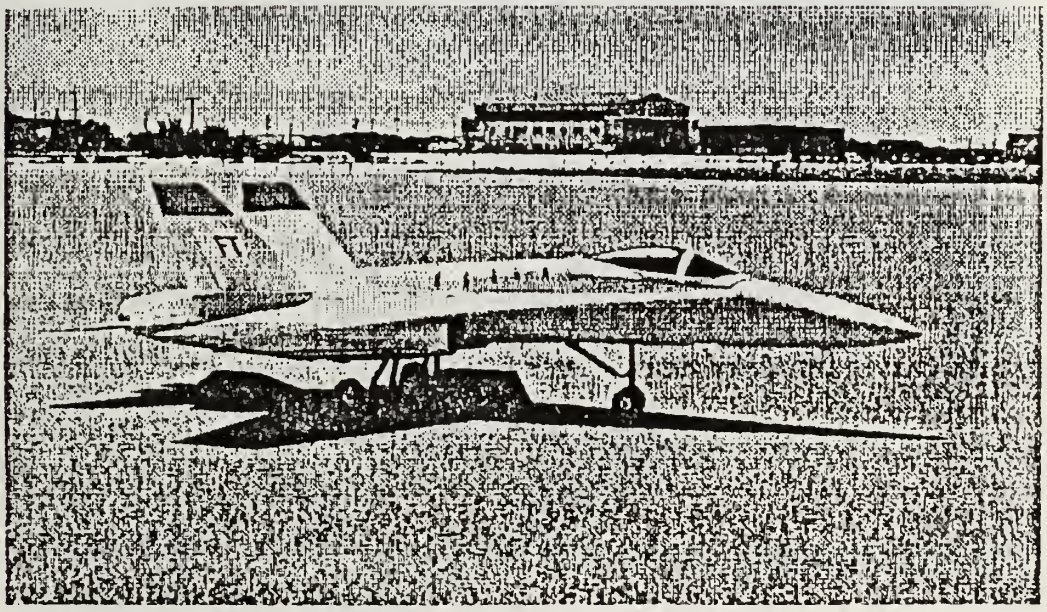

Figure 4 1/7-scale F/A-18 UAV.

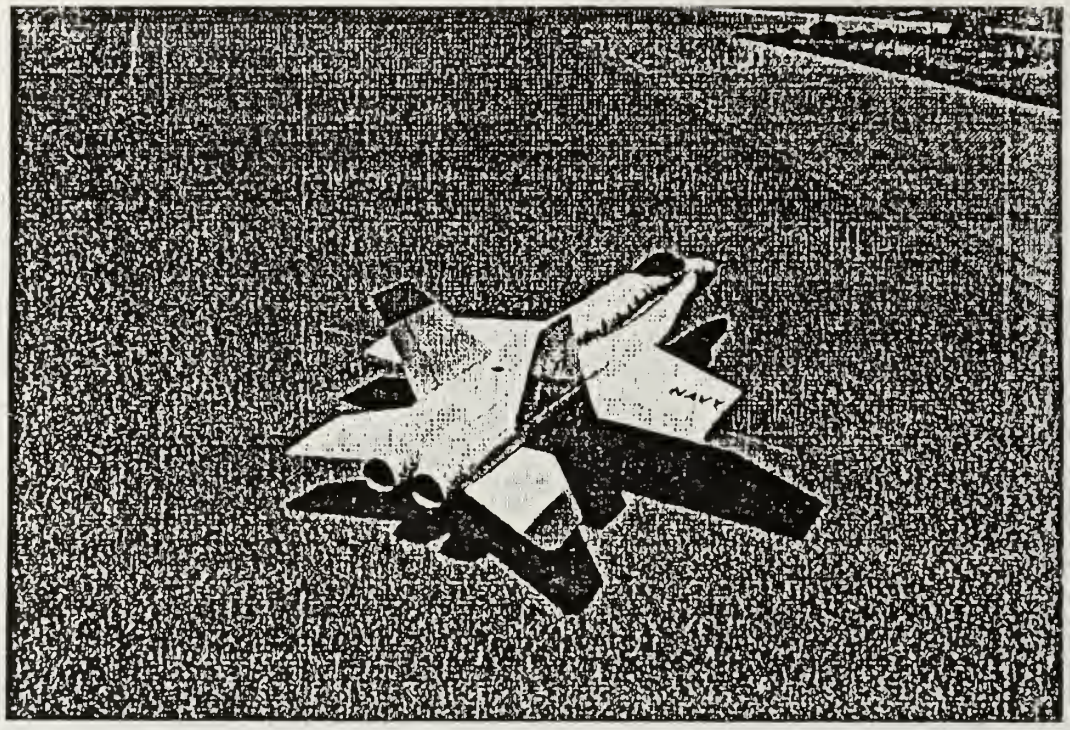

Figure 5 Rear quarter view of F/A-18 UAV.

The kit included the fiberglass components for the fuselage, various doors and panels, tailhook, engine inlet boundary control splitter plates, wing and tail surfaces, and two OS MAX-77 model glow-plug, single-cylinder two-stroke engines to drive Dynamax Ducted Fan Units. The fan units are a joint design by Tom Cook of Jet Model Products and engineers of General Electric, manufactured by General Electric and marketed by Jet Model Products of Raymore, Missouri (Figures 6 and 7).

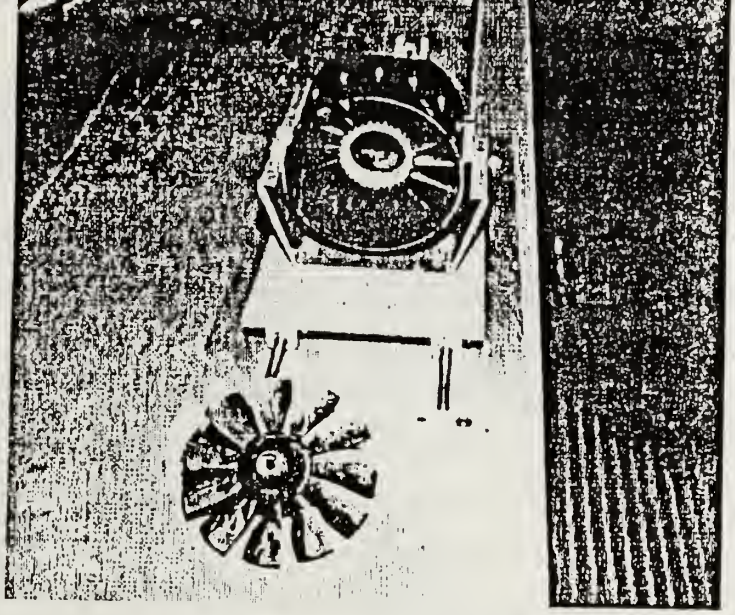

Figure 6 Ducted Fan Unit unassembled (fan and stator housing).

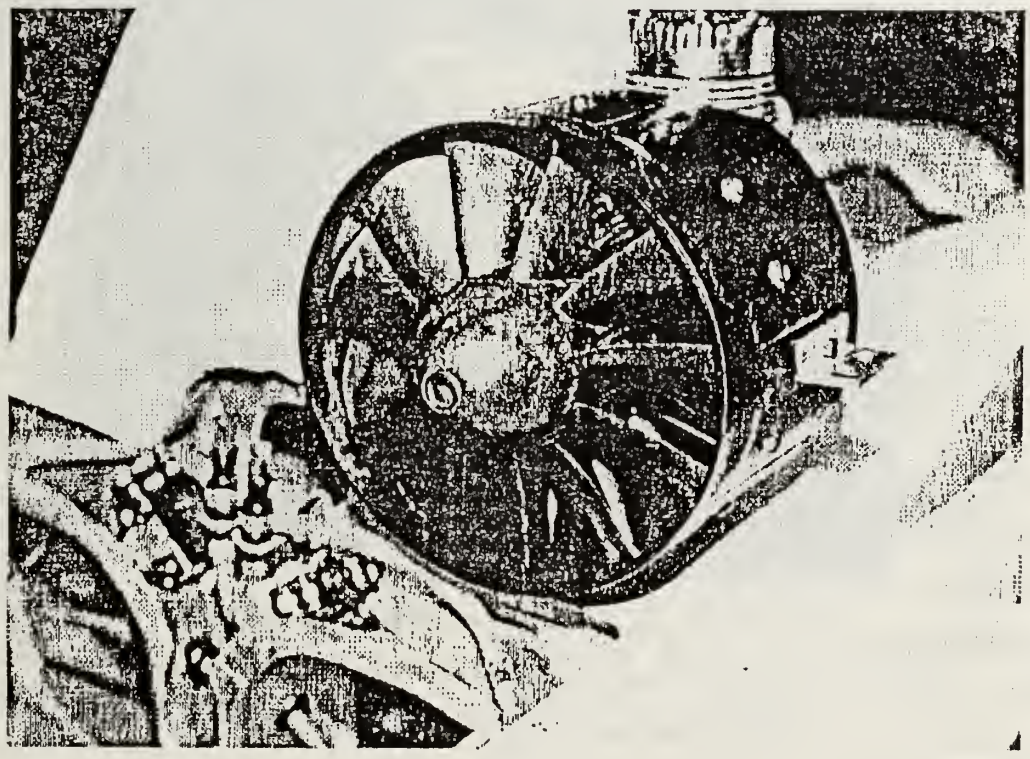

Figure 7 Complete engine-fan assembly.

The engines have since been replaced with a more powerful version, the OS MAX-91VR-DF (Figure 8). They are manufactured by O.S. Engines Manufacturing Company, Ltd., of Osaka, Japan. The OS-91 is externally dimensionally identical to the OS-77, but with a displacement of 0.91 in^3 versus 0.77 in^3. Tables 1 and 2 contain the specifications for the fan units and engines.

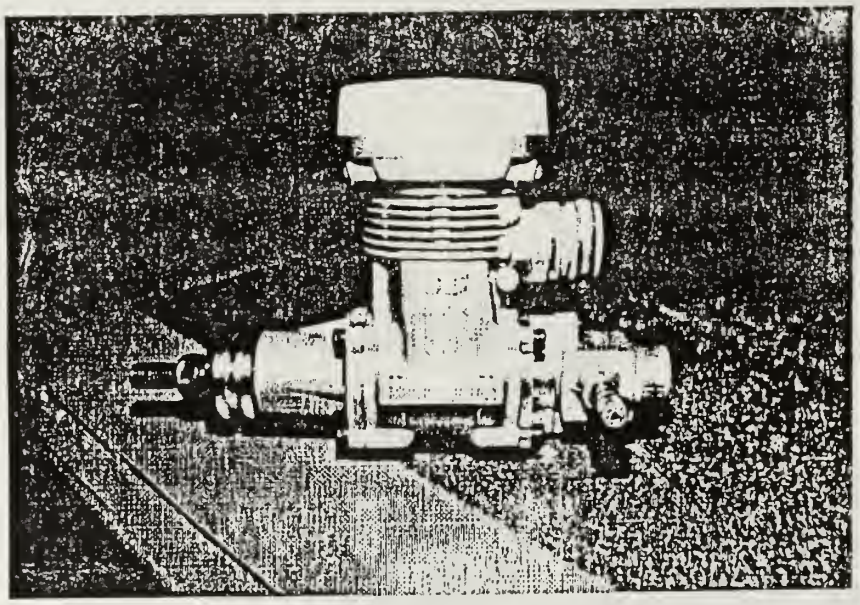

Figure 8 OS MAX-91VR-DF.

TABLE 1

F/A-18 UAV Ducted Fan Units

Fan Model	Dynamax Ducted Fan System
Type	Two-stroke driven, single-stage rotor and stator.
Number of blades	11 rotor, 16 stator
Fan diameter	5 in
Fan hub diameter	2 in
Fan swept area	16.5 in^2
RPM range	As required by engine
Recommended inlet area	20-30 in^2
Recommended tail pipe exit diameter	3.75-4.25 in
Recommended tail pipe length	30 in maximum

TABLE 2

F/A-18 UAV Engines

Engine Model	O.S. MAX-91VR-DF, single cylinder
Carburetor	O.S. Type 9B Automatic
Engine Displacement	14.76 cc (0.91 in^3)
Bore and stroke	27.7X24.5 mm (1.09X0.965 in)
RPM Range	2500 to 25,000 rpm
Power output	4.8 bhp @ 22,000 rpm
Weight	0.662 kg (23.37 oz, 1.46 lbs)
Type glow plug	O.S. #8 or equivalent
Type fuel	Model two-stroke fuel, recommended 5 to 25% nitromethane content.
Exhaust system	Two-stroke tuned-pipe, 18 inch length recommended.

The carburetor is mounted behind the engine on the crankcase, feeding into the crankcase in typical two-stroke fashion. The exhaust manifold is located directly above the carburetor, exhausting straight aft into the tuned exhaust pipe (Figure 9). More than one observer commented on the fact that the carburetor intake faces directly aft, forcing the carburetor intake air to make a 180° turn from the downstream fan exhaust.

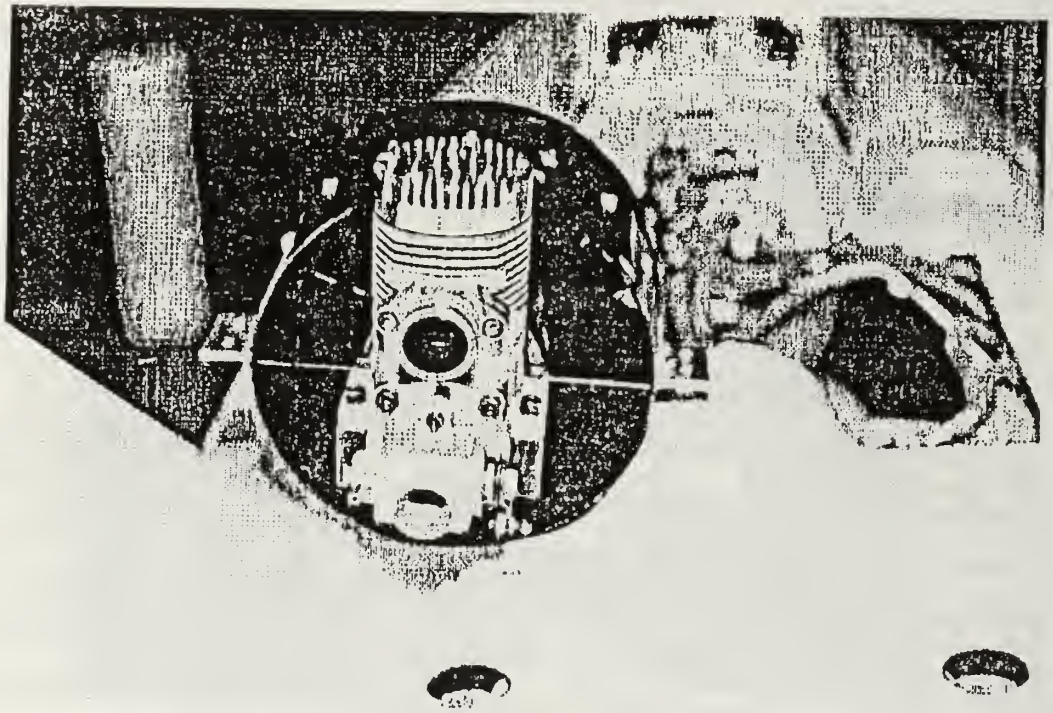

Figure 9 Rear view of the engine.

This appears to present a potential for power loss, but Mr. Mike Callaway of San Jose, California, an F/A-18 UAV program advisor with considerable ducted fan

model experience, said the design works well. He stated a manifold kit is available for attachment to the carburetor intake, with two manifold intakes smoothly bent to face forward directly into the high-velocity fan exhaust to attain some intake ram recovery pressure. However, he recommended not to procure it because of weight and dubious performance gains.

Model construction work that had been completed when the program was taken over included the fuselage sections joined, along with construction of the landing gear and engine-mount boxes, installation of the landing gear, and installation of the horizontal tail and rudder servos. Additionally, to accommodate the Emergency Parachute Recovery System (EPRS), fuselage structural strengthening of the primary wing spar attachment areas and the entire perimeter of the engine bay area had been accomplished. Preliminary parachute drop testing had been completed, along with parachute deployment testing utilizing a cockpit/forebody mockup, made in the shop, atop an automobile at various incidence angles to validate the concept and design.

B. PARACHUTE RECOVERY SYSTEM

Early in the F/A-18 construction program, a wise decision was made to incorporate the EPRS into the model's design. The decision was based on anticipated possible loss of control during high-risk flight maneuvers, possible loss of signal by the receiver, possible structural failure, or other unforeseen mechanical failures. The cost of the kit, additional hardware, new engines, telemetry electronics and sensors and the tremendous amount of man-hours invested dictated the need for a reliable, safe recovery of the model in the event that a landing was impossible. The EPRS needs to lower the model to the ground with minimum damage, essentially preserving the airframe and components

intact for repair and to fly again. This requires also that flight conditions should have little or no wind to alleviate potential drag damage.

Preliminary parachute drop testing had proven the current parachute design inadequate [Ref. 18], and a larger parachute was obtained in November 1990 from the UAV Flight Branch at the Naval Air Test Center in Patuxent River, Maryland. Details of the EPRS design and construction are contained in Appendix B.

C. CONSTRUCTION OF THE MODEL

1. Landing Gear Doors

The model came with detailed landing gear doors, but they proved overwhelmingly difficult to install and operate correctly. The plans and assembly instructions required the use of very small coil springs encased in small wooden boxes to keep the gear doors open and taut against the servo-actuated door retraction lines. However, for the sake of simplicity, picture-frame style flat stock metal springs were utilized to keep the doors open. This was accomplished by bending the springs into the correct shape that gave maximum bonding surface area of the spring against the inside walls of the wheel wells and fuselage. Additionally, the free end of the spring contacting the inside of the gear door was smoothly radiused so it would slide without binding against a plastic strip bonded to the inside of the gear door during operation. The main gear doors had been lined on the inner surface with balsa to stiffen them, and the nose gear door was modified in the same manner. However, the doors remained flimsy and warped readily with any unbalanced closing force, such as the doors being pulled closed against the springs. It was logical to try to mount the spring and door servo control horn as far toward the leading edge of the doors as

possible, which for most of the doors was the only way to do it. The assumption was that, with some warpage almost unavoidable without adding more stiffening weight, one would like to have the door leading edges flush against the fuselage where airstream forces would not be attempting to open the door in flight. It would be acceptable for portions of a door (trailing and side edges) to be open slightly due to warping, but non-flush leading edges would allow ram air pressure to possibly damage or tear off a door.

In fact, although the doors were still quite flimsy, the fuselage areas needed for hinge attachment and spring mounting proved equally poor in stiffness. The final culmination of obstacles occurred during operational checks of the landing gear doors. One of the problems encountered was insufficient servo arm travel to close the doors through their approximately 90^{o} angular displacement, which was solved by increasing the moment arm on the servos and thus the servo throw. However, large stiction and frictional forces of the thin nylon fishing line throughout the servo conduits were encountered to close the doors, which also distorted the fuselage-mounted hinges and springs significantly in some areas. Finally, to continue construction progress on the model, the hinges and springs were removed and the gear doors permanently bonded to the fuselage in the closed position. Cutouts were made just large enough for the landing gear to retract (Figures 10 and 11). This decision was a tough one, for a vast number of construction and troubleshooting hours had been spent on the landing gear doors in an attempt to get them to operate properly in accordance with the assembly instructions and blueprints. The main lessons learned here are that a highly-skilled model builder with excellent craftmanship is needed to carry the construction to a high degree of sophistication, and a much simpler gear door

design should have been implemented from the beginning. The simple cutouts work very well, with no anticipation they will have any significant effect during the high AOA testing that the model will encounter.

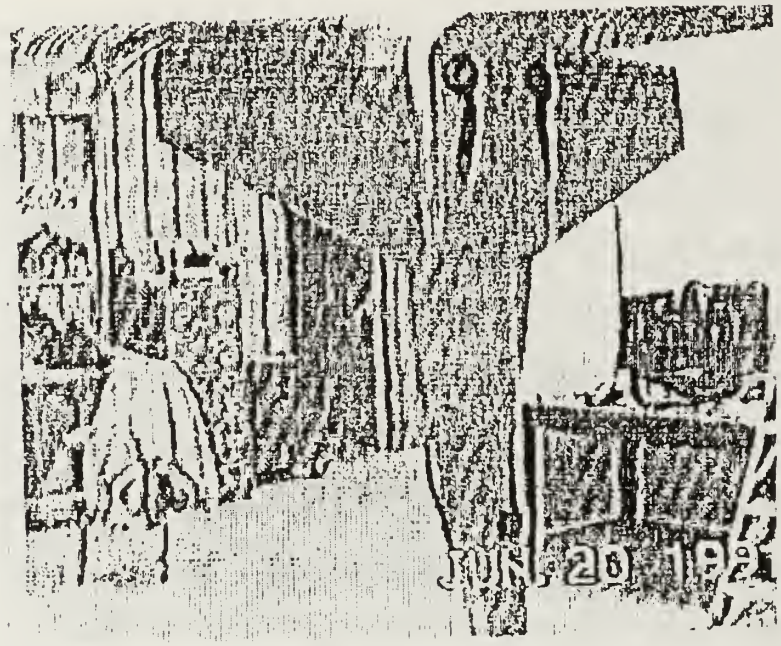

Figure 10 Landing gear cutouts.

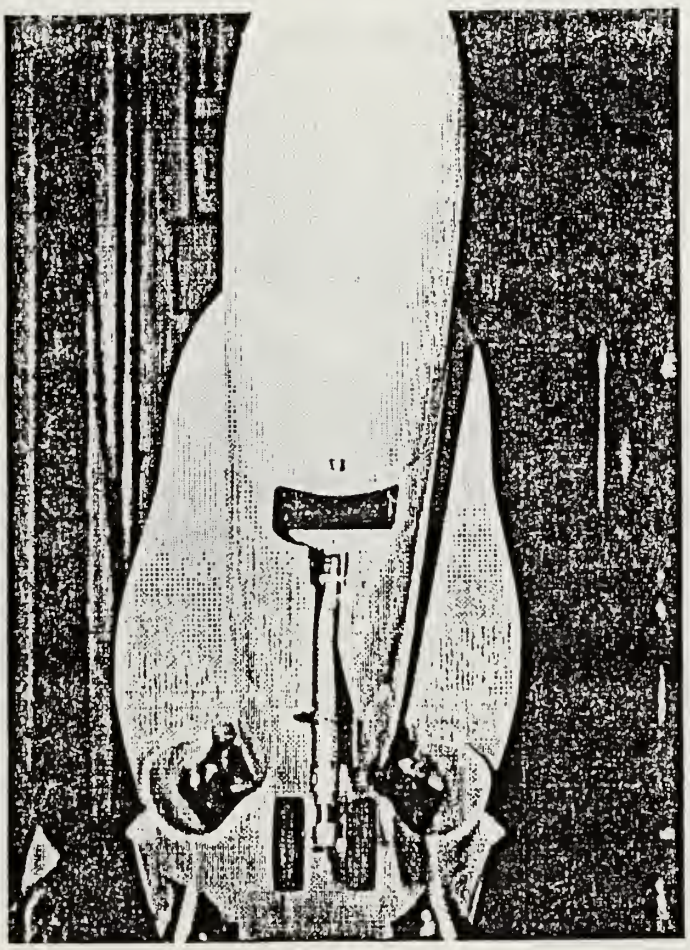

Figure 11 Nose gear wheelwell cutout.

2. Landing Gear

The landing gear is quite detailed for a model, and closely resembles in appearance and operation that of the real aircraft. The main gear has a lightly-sprung rearward-articulating suspension system that uses an oleo strut with no

damping (Figure 12). On deck, the main strut oleo is fully compressed to the stop. The nose gear strut is a conventional telescoping, stiffly-sprung design(Figure 13), and also has no damping. The model's catapult launch bar was not installed.

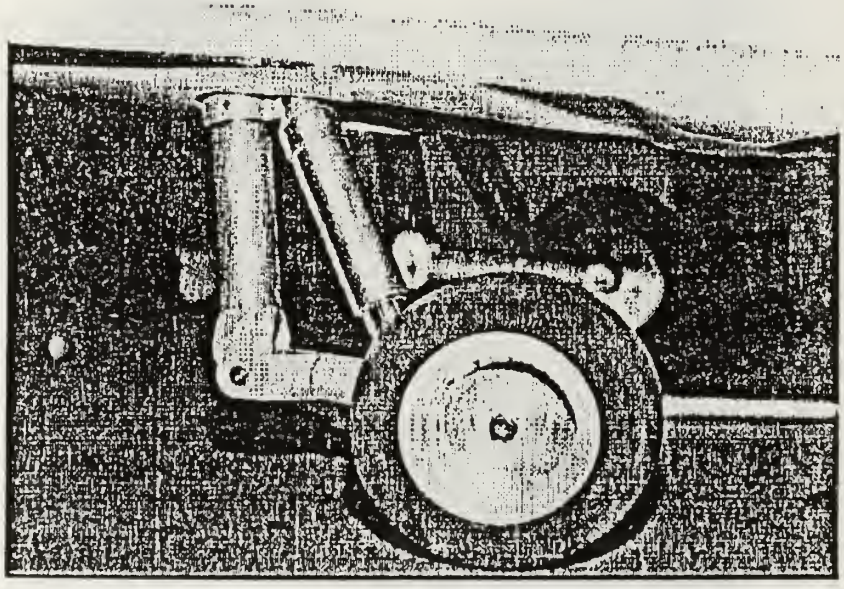

Figure 12 Main landing gear.

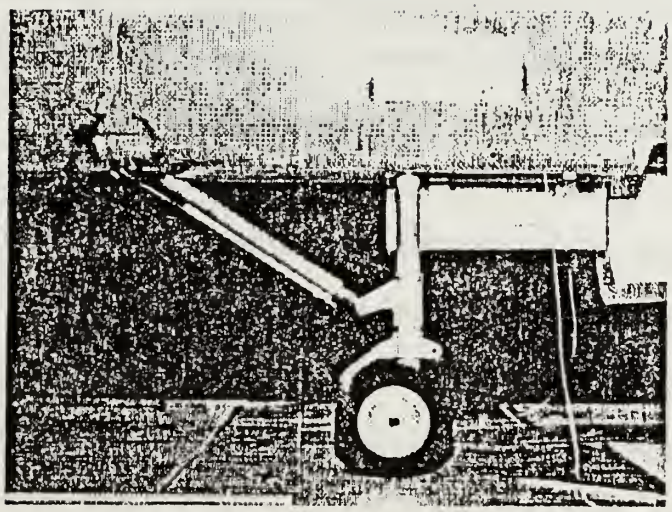

Figure 13 Nose landing gear.

The landing gear works similar to that of the full-scale F/A-18 during retraction and extension cycles, but the hardware quality and oleo design is cheap and poorly manufactured. Both main oleos had tight areas during extension and compression, to the point that when retracted, the gear struts had to be physically pulled into the fully extended weight-off-wheels position in order to fit properly in the wheel wells. This was corrected by disassembling all the landing gear components and individually sanding or lightly machining barrels, pistons and other poorly-fitted parts until smooth operation was obtained. The wheels were each individually fitted to their mounting bolt-axles, then shimmed for correct

endplay and lubricated with dry molybdenum/graphite powder. These procedures consumed a tremendous amount of time, but resulted in a much-improved landing gear system. The geometry of the design does not allow the main landing gear wheels and tires to be fully withdrawn into the confines of the fuselage, but instead the tires protrude approximately one-half inch into the airstream. This is caused by the tires contacting the tail pipe ducts in the retracted position. Before the decision was made to forego the use of operating gear doors, cutouts were employed to allow the doors to fully close.

During landing gear operation, the nose gear retracts forward and the main gear retracts aft, like the actual aircraft. There is virtually no cg change during operation (see Table 4 in the CG and Moments of Inertia section). The nose gear incorporates nose-wheel steering (NWS), operating on the same servo channel as the rudders. The landing gear is pneumatically operated by a servo-controlled valve, supplied by high pressure air from two bottles in the nose immediately forward of the nose wheel well. The bottles are replenished via a threaded Schraeder valve that accommodates a screw-on pump or an ordinary air valve such as found at auto service stations. With air pressure in the range of 60 to 120 psi, each complete cycle of the landing gear (retract and extend) results in approximately a 15 to 20 psi pressure drop. The gear will not completely retract nor extend (that is, with all three uplocks/downlocks firmly in place) when air pressure drops below 35 to 38 psi.

3. Fuel System

The fuel system is divided into identical left and right independent systems, with no crossfeed plumbing incorporated. The fuel is a high-quality model two-stroke type, available in several varieties of nitromethane content. It

is chemically very active and attacks paint; thus it is necessary to use a paint or finish that is impervious or resistant to model fuel. Additionally, lines, seals and other fuel system components must be compatible with model fuel, since it will cause deterioration of components designed for gasoline or other petroleum-based fuels.

a. Tankage

Each system tankage consists of a pressurized 48 fluid-ounce main tank, located just forward of the forward main bulkhead ahead of the engines and immediately ahead of the cg position. A four fluid-ounce feed tank is located inside the fuselage just inboard of the wing attachment area and close to the respective carburetor. Each tank has a weighted fuel pickup "clunker" line that permits all-attitude engine operation, with the exception of extreme nose-down, deceleration conditions when the tanks are partially filled. The most critical case would be main tanks empty and feed tanks below three-quarter to half full, when the feed pickups would likely be uncovered. This may be encountered during a steep approach to landing with the engines throttled back for speed and glideslope control. However, prudent observance of fuel consumption characteristics and strict adherence to maximum flight time schedules should preclude inadvertent airborne fuel starvation.

Each tank was carefully pressure-checked under water for leaks. This is an extremely important item, for the feed tanks are semi-permanently installed and extremely difficult to access in the small space available in the wing shoulders adjacent to the aft engine bay bulkhead. The main tanks are much more accessible. They are located immediately forward of the forward main bulkhead, resting on foam-rubber-covered mounting brackets and held down

securely by a large hook-and-loop strap. However, removal and installation requires the annoying removal of the parachute tray from the cockpit area, the only opening large enough to reach the main tanks (see Figure B-2 in Appendix B).

b. Plumbing

Model neoprene fuel line is used for the plumbing. A neoprene line, used to pressurize the fuel system during operation, is routed from a pressure tap on each exhaust pipe to the upper nipple of the corresponding main tank. This same line serves a secondary purpose as an overflow line during fueling, to vent excess fuel harmlessly into the tuned exhaust pipe, where it is then simply blown out and overboard through the tailpipe during the startup process. This provides a consistent pressurized fuel supply to the feed tanks in all-attitude operation, and also ensures positive fuel pressure for the carburetor. A line from the lower main tank nipple supplies the fuel to the upper nipple of the feed tank, and a line from the lower nipple of the feed tank is routed through a remotely-mounted needle valve, and then to the carburetor. The carburetor has no fuel pump, hence the need for positive fuel system pressurization. The fuel plumbing is quite simple and permits easy refueling/defueling. Labels are attached to each line and recorded to eliminate confusion.

4. Aft Wing Root Step

The model has some design differences from the real aircraft in a few areas, one of them being the wing root design, or the wing/fuselage junction. The actual aircraft's trailing edge flaps' inboard edges are immediately next to the fuselage (Figure 14).

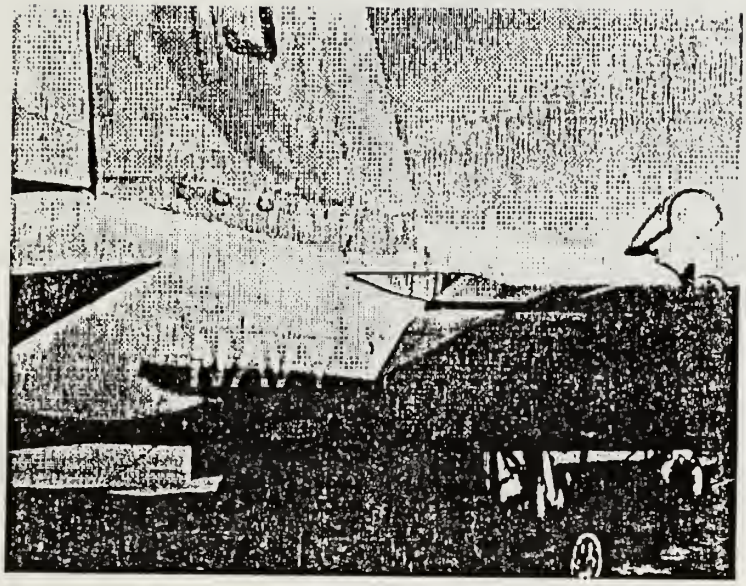

Figure 14 Full-scale F/A-18 TE flap inboard edge.

However, the model incorporates a wing "shoulder" that butts out from the fuselage approximately one half inch (only 1.5 percent of the semi-span, Figure 15). There was a large gap between the wing and fuselage near the wing trailing edge (approximately the flap's chord in length). A 2X2 inch block of balsa wood, called an aft wing step, was cut, shaped and sanded for each side per the instructions to fit into this gap with a smooth, blended contour from the wing shoulder aft into the trailing edge area of the wing (Figure 16). These steps were bonded with 30-minute epoxy, filled, sanded and covered with polyester resin for painting purposes.

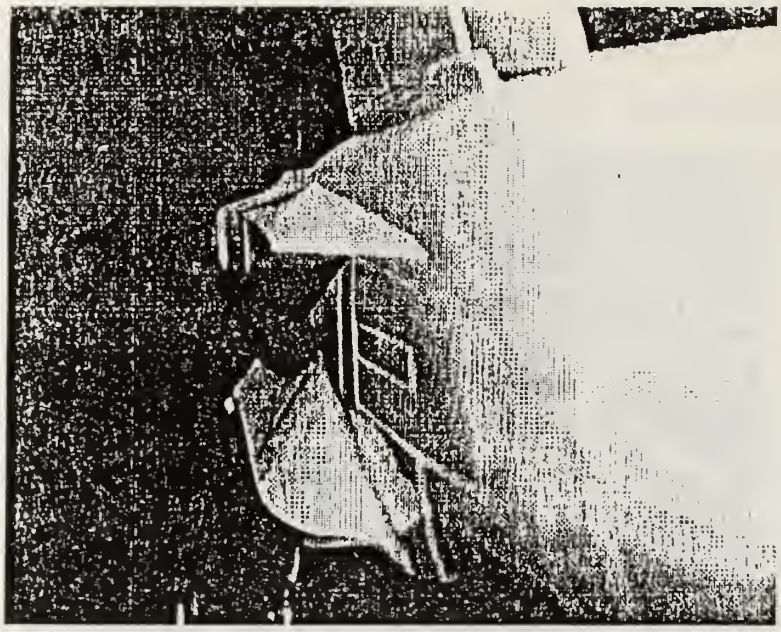

Figure 15 UAV's wing shoulder design.

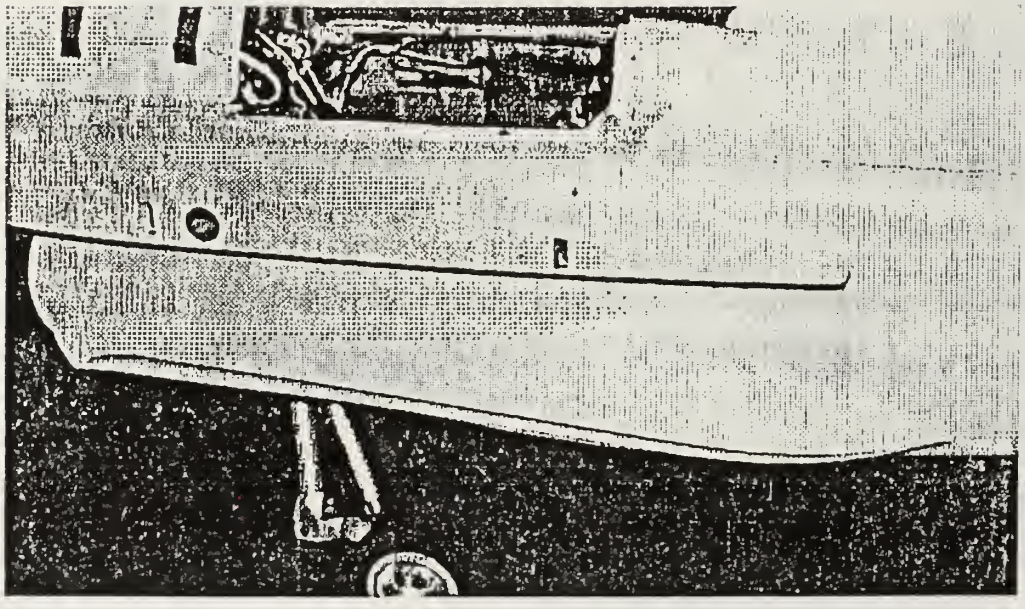

Figure 16 UAV's aft wing step installation.

The model's wings did not come with flaps, but they were incorporated as part of the initial construction [Ref. 18]. It would have been more desirable for the wing to have come with flaps scaled correctly and filling the aforementioned aft wing step space, but such was not the case. This flap design is a significant difference from that of the actual aircraft, but only affects the vicinity of the flaps' inboard edges to the fuselage. This flap design difference is not expected to be a significant factor for the particular high AOA flight research planned for the model (Figure 17).

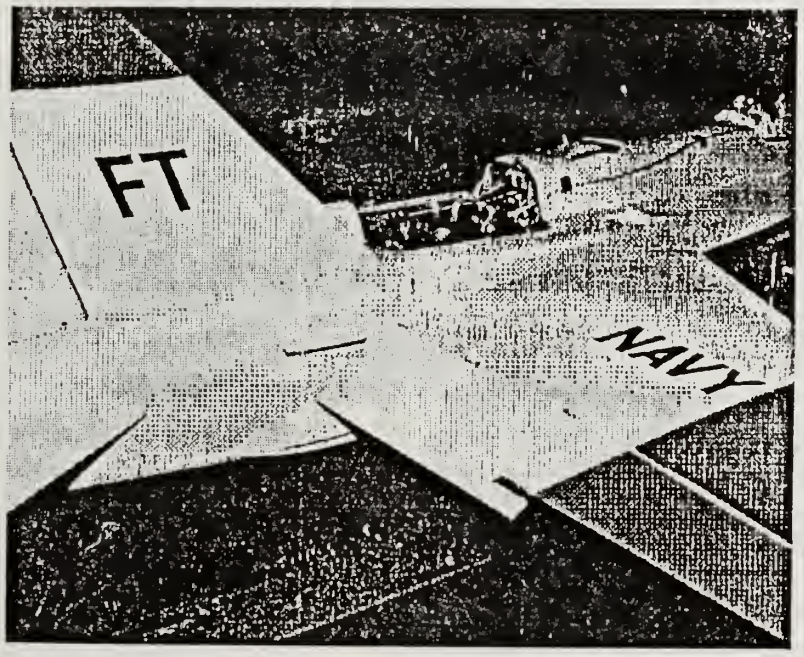

Figure 17 UAV's TE flap inboard edge design.

5. Leading Edge Extensions (LEX's)

The other major model scaling design difference is the size of the LEX's. The model's LEX's (Figure 18) are noticeably much larger in scale than those of the actual aircraft (Figure 19), with span being the biggest deviation. From the leading edge of the LEX to the area where the LEX begins to reflex outward, the scale is identical to the full-scale aircraft. But at the LEX chord point where the LEX semi-span is at its greatest, the model's LEX semi-span is 64 percent that of the adjacent fuselage diameter, whereas that of the actual aircraft is only 37 percent. The model flew quite well on its first and only flight thus far, but the LEX design difference could have some impact in future high AOA research, discussed in Chapter IV [Ref. 22:pp. 399-400].

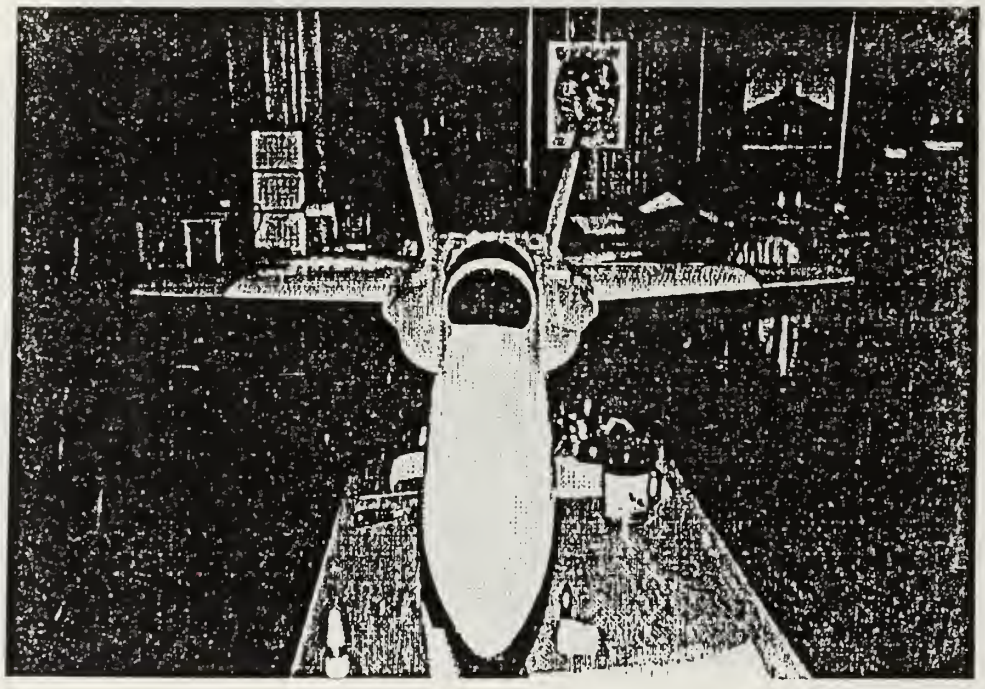

Figure 18 UAV's LEX design.

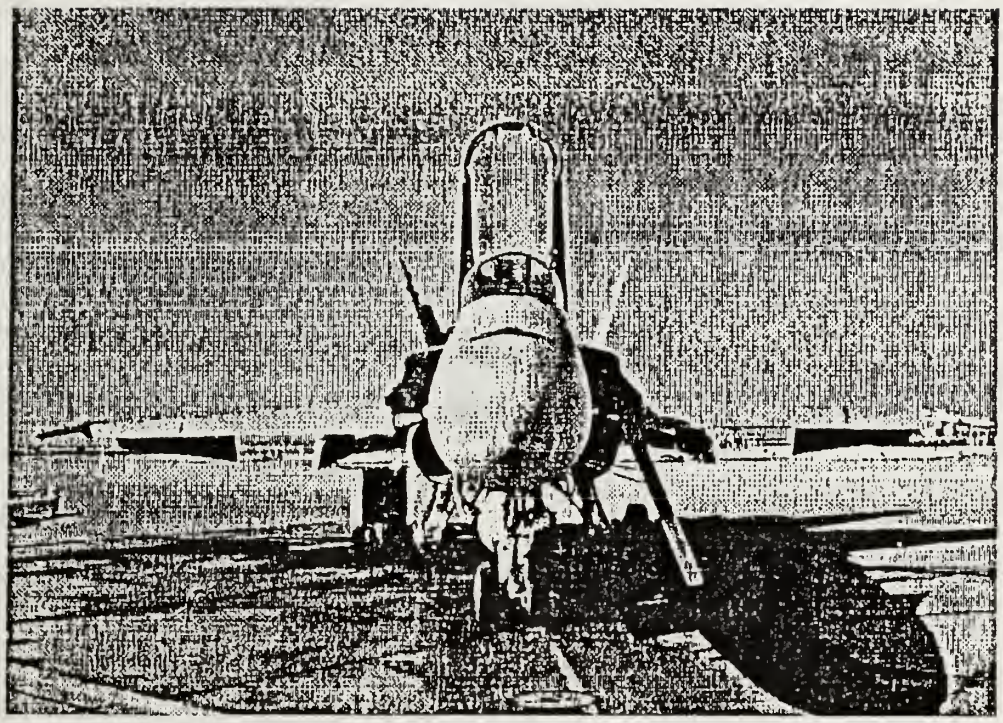

Figure 19 Full-scale's LEX design.

6. Wings, Tails and Flight Control Surfaces

The wings, horizontal stabilizer and vertical tails were constructed of foam core covered with balsa skin [Ref. 21]. The vertical tails came without rudders, but like the flaps, they were incorporated in the initial construction [Reference 18]. The flight controls are actuated with Futaba servos through rod and ball joint or clevis connections. The rudders are synchronized together through a single servo arm. The horizontal tail is all moving. However, the two surfaces are not individually articulated as those on the actual aircraft, but are bolted onto a single shaft that runs laterally through the tailpipes. For flight, the wings are attached to the fuselage by the use of allen head pinch bolts that secure extended wing spars inserted into the wing shoulders (Figure 16). The vertical

tails are permanently mounted, bonded with 30-minute epoxy and the gaps filled with cyanoacrylate (CA) adhesive. Figure 20 is a sketch of the planform of the model's wing. The model, in the interest of saving weight, currently does not incorporate Sidewinder weapon rails and missiles. These items could be installed at a later date, once the model has more flights and only if the rails and missiles, with their associated extra weight and drag, are deemed to be essential to the research effort. However, long-range plans likely will place a swiveling-head airspeed transducer assembly in one of the wingtips, making it unlikely that the Sidewinder rails and missiles would be installed. A wingtip would be the safest place to install an airspeed transducer to provide the least amount of risk of possible parachute entanglement in the event the EPRS is activated. Figure 21 shows the geometric relationships used to determine the 1/4-chord wingsweep angle $\Lambda_{1/4}$ from Equation 1. Table 3 contains specifications of the completed aircraft.

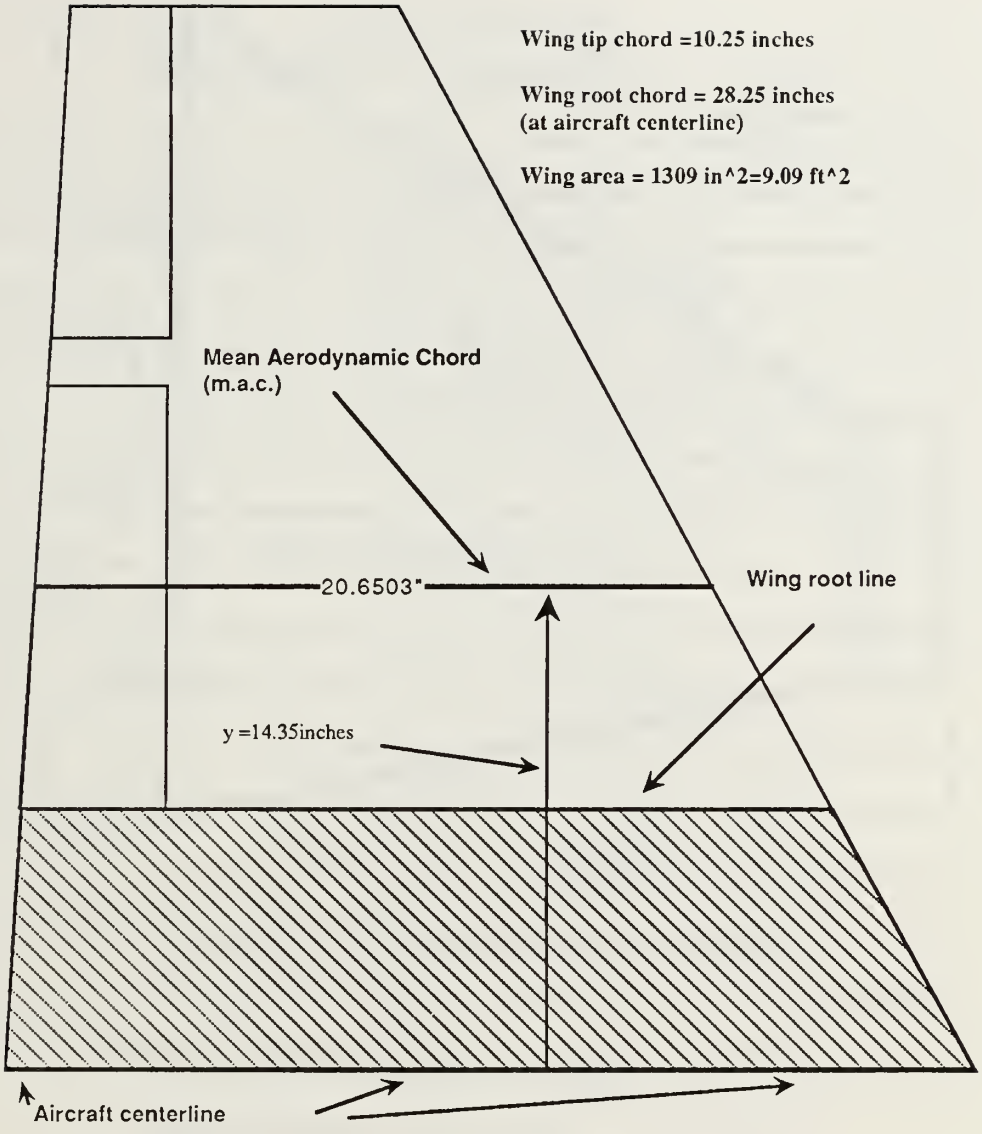

Figure 20 F/A-18 UAV wing.

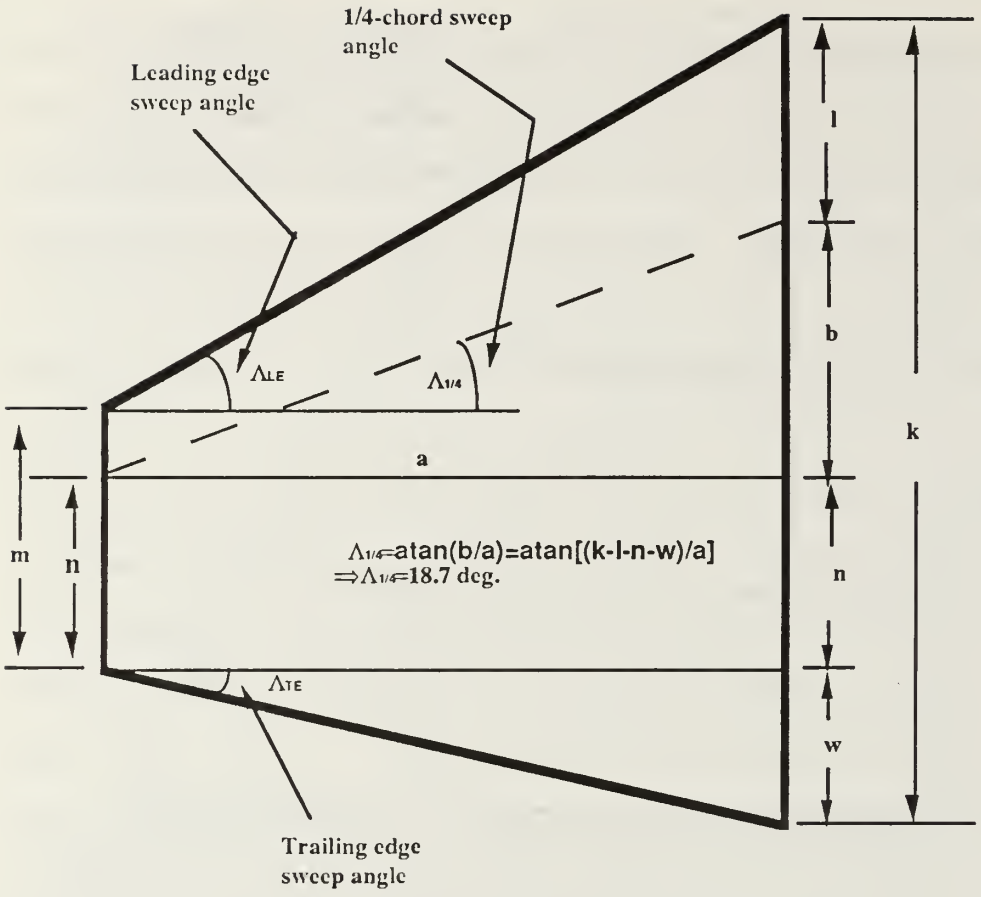

Figure 21 Geometric relationships for determining wingsweep angle.

TABLE 3

General F/A-18 UAV Dimensions

Length	8 ft 2 in --- 98 in
Wingspan -- b (without SW rails)	5 ft 8 in --- 68 in
Height	2 ft 2 1/4 in -- 26 1/4 in
Weight (Full / empty)	31.55 / 28.89 lbs
Fuel load	Approx. 2.7 -3.0 lbs
Wing area -- S	9.09 ft^2 --- 1309 in^2
Aspect ratio -- AR	3.532
LEX area -- S_{LEX}	1.02 ft^2 --- 146.25 in^2
Horizontal tail area -- S_{ht}	1.82 ft^2 --- 262.4 in^2
Vertical tail area -- S_{vt}	2.16 ft^2 --- 310.9 in^2
Aileron area -- S_a	0.51 ft^2 --- 73.1 in^2
Flaps area -- S_{fl}	0.81 ft^2 --- 117.0 in^2
Rudder area -- S_r	0.52 ft^2 --- 75.3 in^2
Leading edge sweep angle -- Λ_{LE}	25.2°
Trailing edge sweep angle -- Λ_{TE}	-3.4°
Wingsweep (1/4 chord) -- Λ	18.7°

7. Engines and Ducted Fan Units

New OS-91 engines were received in November 1990 and were then delivered to Mr. Callaway for teardown, inspection and a careful "blueprint" rebuild. Ducted fan engines typically turn in excess of 20,000 to 22,000 rpm at full throttle. According to Mr. Callaway, who has extensive ducted-fan model experience, ducted-fan engine longevity is a direct function of careful assembly, adjustment, proper balancing and matching of internal parts, and proper break-in

procedures. In addition to inspecting the engines, he has provided consultation for the flight program and piloted the first flight. Eventually, flight tests of the model will be conducted in-house with the UAV Lab's own Lab Technician and highly-experienced R/C model pilot.

a. Engine Break-In

After engine reassembly, the engines were broken in using an engine stand, shown in Figure 22. All engine testing and the first flight utilized the 16-1/8-inch long tuned exhaust pipes supplied with the original OS-77 engines.

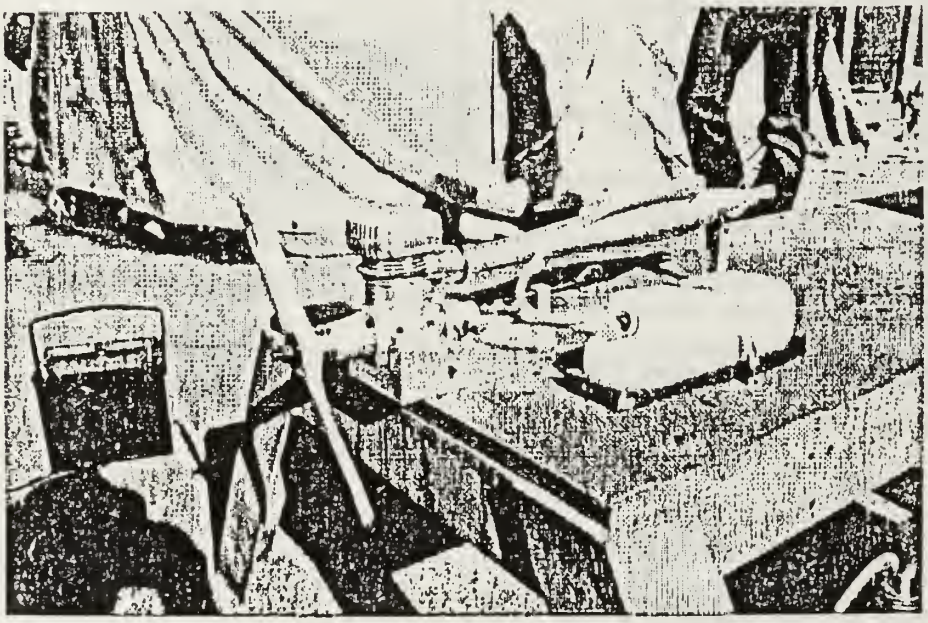

Figure 22 OS-91 engine on the break in stand.

These pipes have an 11/16-inch diameter inlet and 3/8-inch diameter outlet. Discovery was made after the first flight that longer pipes (18 inches) are available for OS-91 operation with the Dynamax Ducted Fan Units, which will be procured for further flight testing. The breaking-in process used a 10-inch diameter wooden propeller mounted to the engine to limit engine speed to approximately 16,000 rpm. Each engine required approximately 1-1/2 operating hours for proper break-in, and to permit proper adjustment of idle mixture and needle valve settings for good throttle response and a stable idle. Three 48-fluid ounce tanks of five percent nitromethane model fuel for each engine were consumed. The OS-91 engine brochure and operating instructions do not specify a maximum allowable nitromethane content, although it does recommend using five percent for break-in purposes and ten percent during initial flights. Word-of-mouth guidelines call for a range of five to 25 percent nitromethane during operation. The operating instructions address the use of higher nitromethane mixtures if more power is required, but also cautions the operator about the increased wear and shortened engine life with the use of higher nitromethane content mixtures at high power. Two ounces of lubricating castor oil are normally mixed per gallon of fuel.

b. Engine Thrust Testing

After break-in, an engine test stand (Figures 6 and 23) was used to determine maximum thrust of one of the engines. A test tailpipe was fashioned from a 36-inch length of metal heating duct. The duct was shaped to the same diameter as the model's tailpipes, and was held in the correct shape by plastic zip-ties.

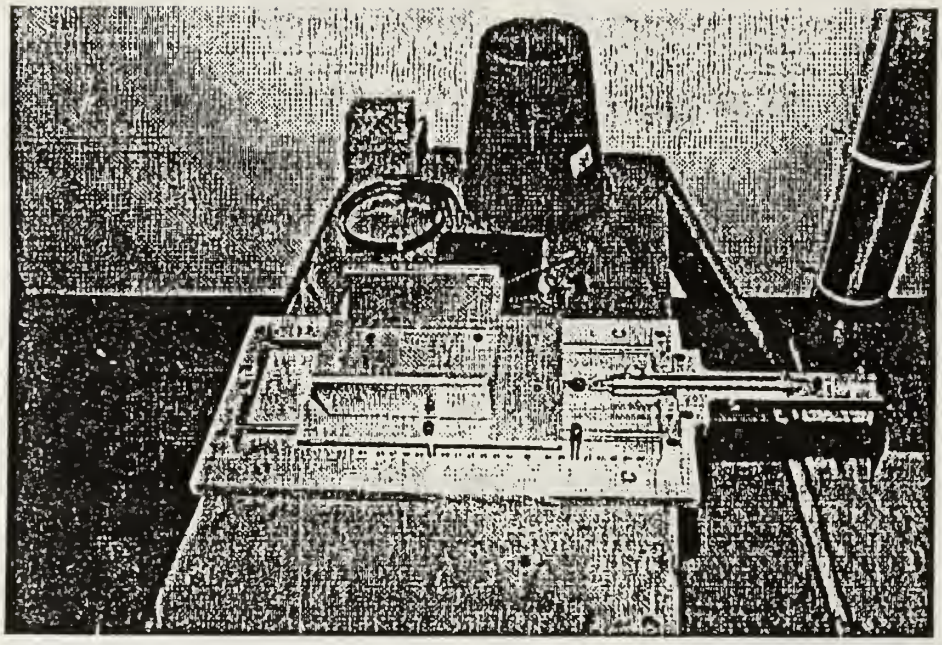

Figure 23 Engine thrust stand and apparatus.

The upper, forward part of the pipe was cut out to fit around the cylinder fins, and a foil cap made to cover the head and provide proper cooling airflow to the head during operation. The head was the large-head type, which is normally used in non-ducted fan applications, and are unsuitable for the F/A-18 model's engine bay because of lack of room. However, they proved adequate for thrust testing. The heads were later milled down to the proper small-head dimensions, and factory small heads were later obtained through the purchase of two more OS-91 engines, to be used as spares.

Very thin shims were required to ensure proper alignment of the fan inside the stator housing as the engine was bolted to the fan unit. After mounting and assembly of the engine, tail pipe and all fan components, the entire apparatus was bolted to the upper portion of the engine thrust stand. During thrust testing, the upper portion slides on guides of the test stand base (Figure 23). A spring assembly with scale and pointer were mounted to the base and attached to the upper portion of the test stand. The aft part of the tailpipe was supported on a soft drink can that rolled freely during longitudinal motion of the engine assembly and upper thrust stand. Unfortunately, no photograph is available of the complete ready-to-run thrust test configuration on the thrust stand.

For the first thrust test, the engine was run without any intake ducting or attempts to smooth the airflow into the mouth of the fan housing. After careful needle valve adjustment, a consistent maximum thrust of almost 9 lbs was obtained at 21,200 rpm. As an experiment, the bottom of an ordinary child's sand bucket, seen in Figure 23, was cut out and the bucket secured by a large hose clamp to the mouth of the stator housing, forming a rudimentary but effective bellmouth. Maximum thrust increased to 11-1/4 lbs at 22,500 rpm with this modification alone. Although the bellmouth does not resemble the model's actual intake and is much larger in intake area, it does provide smoother airflow, just as the model's intakes do. Maximum installed static thrust with both engines has not been determined, but is estimated to be 21 to 22 lbs.

An earlier idea to conduct thrust testing with two stator blade configurations (all installed and half removed) was discarded based on the recommendation of Mr. Tom Cook of Jet Model Products, Inc. [Ref. 23]. The

idea to test the two configurations came from a common assumption that removal of half the blades would reduce stator blade blockage and increase thrust. However, removal of the blades could also increase the swirl component of the downstream air from the fan and negate any advantages of the fewer stator blades in the fan exhaust. Mr. Cook's main concern was for structural integrity and safety, and he stated the Dynamax Fan Units were designed and thoroughly tested with the help of General Electric engineers. His contention was that the fan units were already operating at optimum performance, as designed. This writer concurs with the recommendation that anyone employing the use of Dynamax Fan Units not remove any of the stator blades in the quest for increased thrust.

8. Prep and Painting

The model took approximately 25 hours to sand and prep for painting. Much of this time was spent filling cracks and crevices and smoothing of discontinuous fuselage sections with plastic body putty. There was a big problem with the forward fuselage area, which had been sprayed with mold release agent to facilitate serving as a mold for a forward fuselage and cockpit mockup for the EPRS deployment testing [Ref. 18:pp. 43-53]. The mold release agent was extremely difficult to remove, and had soaked into some of the porous areas of the fiberglass. This manifested itself during painting, for the paint puckered and beaded wherever there was mold release. Several cycles of cleaning with paint thinner and reapplication of the white enamel paint finally resulted in an acceptable finish, but some areas still needed final touching up by brush. The wings and tail surfaces were covered with white mylar sheet vice fiberglass to save weight, with the tip areas covered with fluorescent orange mylar sheet.

9. Internal Components

After painting was complete, final installation of plumbing, wiring and and major hardware items was accomplished. Futaba servo Y-connectors and wiring were routed and secured with small plastic ties. Any area of potential vibration and chafing was reinforced, padded and securely tied off. The engines were installed and the exhaust pipes were mounted. Holes cut into the top of the aft fuselage above the tailpipes facilitated the installation of the fuel system pressurization lines through grommets in the top of the tailpipe ducts onto the pressure taps of the exhaust pipes. These holes are plugged with solid rubber grommets for flight. Parachute packing training of other personnel was conducted, and the parachute installed. Final fit and security checks were made via a thorough quality assurance inspection. All plumbing and wiring was tagged and recorded.

D. OPERATIONAL CHECKOUT

To operate the servos for the various systems, a Futaba nine-channel receiver commanded by a Futaba 1024A transmitter is utilized. Its nine channels are powered by a 9.6 volt 1200 mah battery, and hooked up to the ailerons (Y'd into one channel), flaps, throttles (Y'd into one channel), rudders/NWS, elevator, landing gear and EPRS release servo.

1. Landing Gear

The landing gear was cycled approximately 40 times to check for any interference with the cutout areas and any internal components. The nosewheels displayed a disturbing propensity to become cocked while in the up position when the aircraft was vibrated. This caused the nosegear to hang up in the wheelwell and prevented it from extending with the rest of the landing gear

when lowered. A guide was installed to prevent this binding. Initial leakdown tests of the landing gear air supply revealed about a 1.5 psi/min loss, which was traced to a dry and cracked O-ring on the pump fitting and not attributable to the landing gear pneumatics. The tests also revealed that 35-38 psi was the very minimum needed to cycle the gear up and down one time. Any less pressure would not seat the downlocks or uplocks into position. A minimum pressure of 60 psi has been established for flight.

2. Parachute Hookup

The parachute risers are two 400-pound test, flat nylon lines that emerge from the rear of the cockpit and are taped flat against the outside of the fuselage with small strips of duct tape. The ends are secured to 220-pound strength Quick-Links which are attached to mounting brackets on the aft side of the forward bulkhead, inside the engine bay. The engine bay hatch covers the risers, and will likely be torn free if the parachute is deployed. Since the maximum design load on the risers is approximately 50 pounds [Ref. 18:pp. 39-40], a pull test to approximately 60 pounds was conducted on the attachment points, Quick-Links and risers. The model has an estimated nose-up attitude of 15° to 20° when suspended from the attachment points. The receiver was programmed via the Futaba 1024A transmitter to operate in a fail-safe mode if loss of transmitter signal occurs for more than 2 seconds, whereupon the canopy releases while simultaneously closing the throttles. This is easily checked on the ground by turning the transmitter off while the aircraft power supply is still turned on.

3. Flight Controls

The flight controls were exhaustively checked. Initial testing revealed that one aileron and one flap were rigged backward. The aileron was easily fixed by rotating the servo arm 180°, but the flap's servo arm and rod proved too difficult to reengineer and fit in the available space. Thus, each flap was given its own channel. The two channels are mixed via controls on the Futaba 1024A transmitter, allowing the single rotary flap switch to operate the flaps in unison. Each surface is adjusted electronically via the transmitter for throw and neutral position. Because of this, the flaps can actually be rigged with any amount of droop in the full UP position. If another channel were available, the ailerons could be rigged slightly TEU or TED (droop) for a neutral position, which would add flexibility to future high AOA research. This could actually save redesign effort in the future if all the flight controls are reconfigured to be individually articulating, commanded by a flight control computer. The assembly instructions do not address where to place the neutral position of the horizontal stabilizer (stabilator). Based on the placement of the c.g. (see next section) and experienced advice, a neutral position of approximately 3° TEU was established, which proved satisfactory for the flight. The stabilator can be trimmed approximately ±4°. The throw limits of the horizontal tail and ailerons can be adjusted electrically via the transmitter to provide HIGH and LOW sensitivity settings (i.e., LARGE and SMALL surface throws) as appropriate for each phase of flight.

The rudders are mechanically synchronized and electrically Y'd together with NWS. The rudder/NWS throw limits can also be electrically

adjusted to reduce the sensitivity of directional control during taxi, takeoff and landing.

The horizontal tail surfaces were balanced, for flutter prevention, with lead weights inserted into the inboard edge of their foam cores. The weights were then epoxied into position and taped over.

E. CENTER OF GRAVITY, MOMENTS OF INERTIA AND AERODYNAMIC PARAMETERS

1. Center of Gravity

The F/A-18 UAV was weighed empty and with full tanks. The cg was determined with the use of Equation 2 [Ref. 24], where W_F was the weight on the front support, W_R was the weight on the rear support, and $\bar{l}$ was the distance between the two (Figure 24). Equation 3 [Ref. 24] could be used for a fixed-gear aircraft, or where jack supports are available for retractable-gear models, with W_1 the weight on the left gear/jack, W_2 the weight on the right one and W_3 the weight on the forward support or nosegear (Figure 24). In the figure, $\bar{l}$ is the distance between W_3 and a line drawn between W_1 and W_2. x_{cg} was the distance forward of the rearmost reference jack point (W_R in this case) and was marked on the aircraft. This mark was then translated outboard to intersect the m.a.c. line drawn on the wing, and the cg was then defined in terms of percent m.a.c. ($\bar{c}$). A single weight scale was utilized, measuring each end of the aircraft while the other end was supported in a level attitude. Equation 2 was used vice Equation 3 because the rearward pivoting of the lower part of the main landing gear while sitting on deck would cause an inaccurate measurement of the length $\bar{l}$ in the determination of the gear-down cg. To keep it simple, a single support at each end was used so that the cg determinations could be more easily made with

the gear up and down. Center of gravity results are shown in Table 4. In each case, the cg shifted forward slightly as the landing gear was raised. The assembly instructions and plans locate the design cg exactly at the forward bulkhead, which results in a design cg of 15.1% m.a.c.

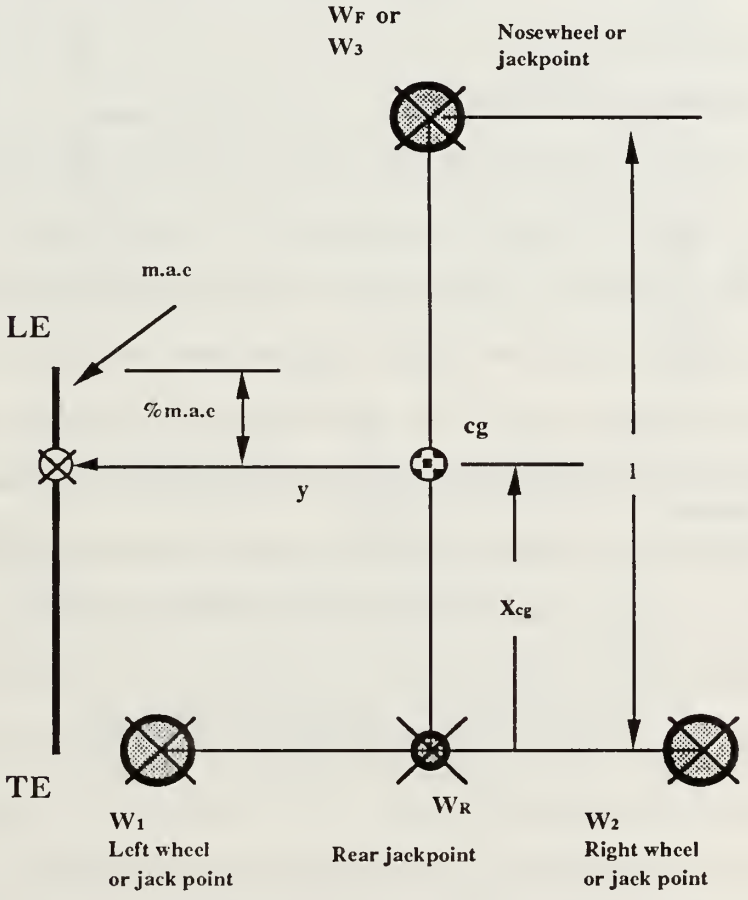

CENTER OF GRAVITY DETERMINATION

Figure 24 Center of gravity determination.

The m.a.c. was determined from Equation 4, where λ is the wing taper ratio defined in Equation 5. The m.a.c. of 20.65 inches and taper ratio are found in Table 4. As one may note, the four calculated cg's of the actual model are slightly aft of the design point, although still quite forward of the quarter chord

point, and very likely well ahead of the stick-fixed neutral point, which has yet to be determined. As a note of interest, m.a.c., or $\bar{c}$, is located on the wing by precisely placing the calculated m.a.c. line on the leading and trailing edges of the wing. Equation 6 assists in locating $\bar{c}$ out from the centerline of the model (note Figures 20 and 24).

2. Moments of Inertia

The aircraft moments of inertia were determined in accordance with Equation 7 [Ref. 24], where P is the period, a is the diameter of a circle scribed by the suspension lines, L is the length of the suspension lines, W_{MS} is the weight of the suspended mass and supporting hardware and W_S is the weight of the supporting hardware (Figure 25). The moments of inertia were determined with an empty model only because of the possibility of fuel leaks in the unusual attitudes involved. Total weight of the lines and supporting hardware for the moments of inertia testing was only 2 ounces (0.43 percent of the total weight); thus the term of W_S in Equation 7 was ignored. The aircraft was suspended by two 400-pound strength nylon lines, length (L) 104 inches long and diameter (a) 64 inches at the suspended points of the model. The model was suspended upright for yaw moment of inertia determination (Figure 26) and on its side for pitch of moment of inertia. For roll moment of inertia, the model was suspended nose down (Figure 27), hanging from the horizontal tail shaft, with a line length (L) of 40 inches and diameter (a) of 13.5 inches.

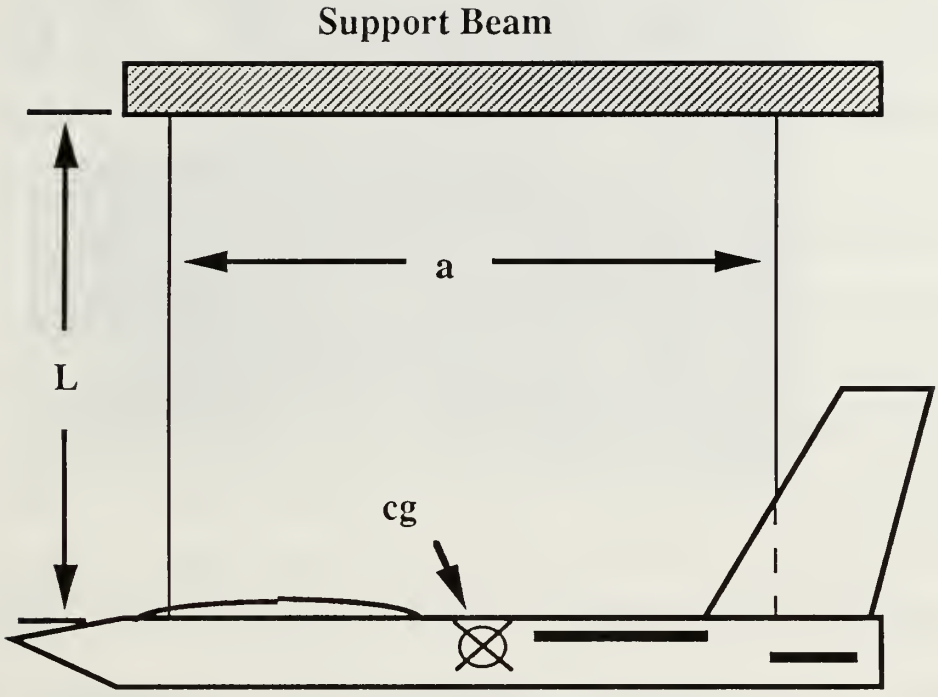

Figure 25 Schematic for determining moments of inertia.

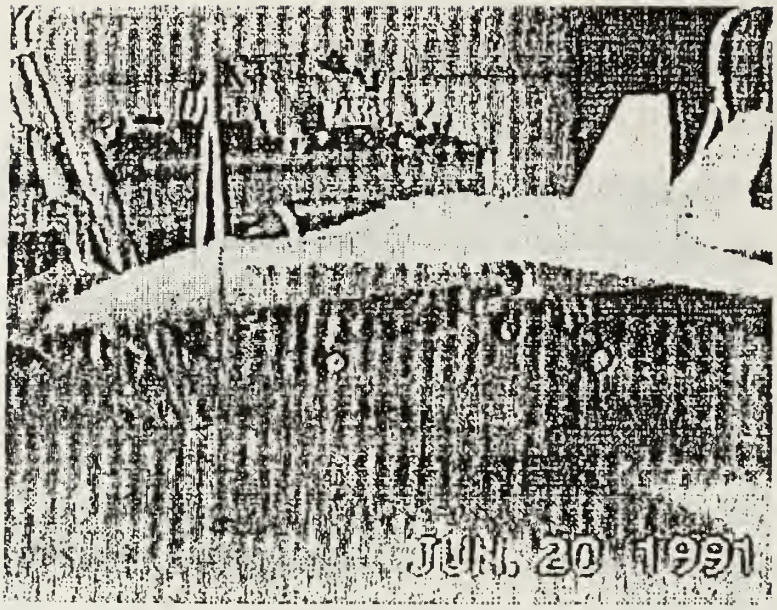

Figure 26 Model suspended for yaw-axis moment of inertia (gear extended).

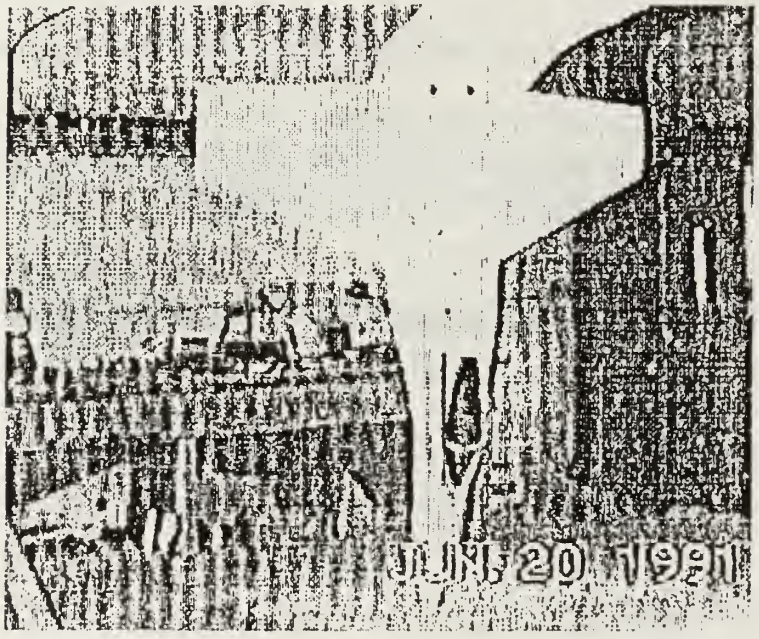

Figure 27 Model suspended for roll-axis moment of inertia (gear retracted).

After the model was hung, ensuring the suspended points were equidistant from the cg, it was displaced a small angular amount of about 20° to 30°, then released and the period of the oscillations recorded. The particular method employed was to time 10 complete oscillations and then determine the period by dividing by 10. This was repeated twice more in each of the three axes in order to establish a statistical average. The results of the moments of inertia testing are shown in Table 4. For comparison, data for the full-scale F/A-18 are shown in Table 5 [Ref. 25 and 26]. Of interest is the value of the Roll/Pitch Inertia Ratio (I_{xx}/I_{yy}). Both values for gear retracted are very close, 0.158 and 0.184 (16 percent difference) for the 1/7-scale model and the actual aircraft, respectively. This characteristic will be discussed in further detail in the next chapter.

The values for horizontal tail volume and vertical tail volume are listed in Table 4 and were determined from Equations 8 and 9, respectively. Tail volumes (also known as tail volume ratios) are a measure of the power of the tail and are directly related to static and dynamic stability. More will be discussed on these parameters in the next chapter. The m.a.c. of the horizontal and vertical tails were computed in a manner exactly as was done with the wing m.a.c., using Equations 4 and 5.

TABLE 4

Aerodynamic and Dynamic Data

Wing loading (full fuel) -- W/S	3.471 lbs/ft^2	
cg (% m.a.c.)	Gear Down	Gear Up
Empty	16.82	16.60
Full	16.38	15.58
Mean Aerodynamic Chord (m.a.c.)	1 ft 8.65 in --- 20.65 in	
Taper ratio -- λ	0.3628	
Wing tip chord -- c_T	10.25 in	
Wing root chord -- c_R	2 ft 4.25 in --- 28.25 in	
Moments of inertia (empty)	Gear Down	Gear Up
I_{xx} (Roll) lb-ft-sec^2 -- slug-ft^2	0.316 -- 0.00982	0.281 -- 0.00873
I_{yy} (Pitch)	1.731 -- 0.05381	1.776 -- 0.05520
I_{zz} (Yaw)	1.807 -- 0.05618	1.862 -- 0.05787
Roll/Pitch Inertia Ratio -- I_{xx}/I_{yy}	0.183	0.158
Aircraft deck angle	5 1/2 ° NU	
Control surfaces travel		
Ailerons	Right 37° TEU, 29° TED	
	Left 28° TEU, 29° TED	
Horizontal stab	12° TEU, 15° TED	
Rudders	± 22°	
Flaps	39.5°	
Horizontal tail length -- l_t	2 ft 8.75 in --- 32.75 in	
Horizontal tail volume -- V_H	0.3179	
Vertical tail length -- l_F	1 ft 9 in --- 21 in	
Vertical tail volume -- V_F	0.0734	

TABLE 4 (continued)

m.a.c of horizontal tail -- c_{HT}	11 in
m.a.c. of vertical tail -- c_{VT}	12.25 in
Horizontal tail taper ratio -- λ_{HT}	0.4483
Vertical tail taper ratio -- λ_{VT}	0.4198

TABLE 5

McDonnell Aircraft F/A-18 Hornet Specifications

(Based on a weight of 32,550 lbs., 60% internal fuel, cg at 22.1% m.a.c., two AIM-9's on wingtip stations 1 and 9, two AIM-7's on fuselage stations 4 and 6)

Length	56 ft
Wingspan (without missiles)	37 ft 6 in
Height	15 ft 3 in
Empty operating weight	24,500 lbs
Internal fuel capacity	10,800 lbs (JP-5)
Maximum speed (at 20,000 feet)	725 KCAS/1.5 Mach
Stall speed (2000 lbs. fuel) Power off Military thrust	 108 KCAS 86 KCAS
Moments of inertia I_{xx} (Roll) I_{yy} (Pitch) I_{zz} (Yaw) I_{xz}	lb-ft-sec^2 (slug-ft^2) 23,196 (721) 126,092 (3917) 145,340 (4517) -3115 (-97)
Roll/Pitch Inertia Ratio -- I_{xx}/I_{yy}	0.184

F. FIRST FLIGHT

1. First Flight and Results

The F/A-18 UAV made its first flight on 29 June 1991 at Fritzsche Army Airfield at Fort Ord, California. The flight was planned for four minutes, and lasted 3 minutes and 40 seconds. The weather was clear and windy, at 10 knots with gusts to 16 knots, approximately 15° left of centerline of the duty runway. Mr. Mike Callaway was the pilot. The fuel used was a 50-50 mix of 10 and 25 percent nitromethane, yielding a 17-1/2 percent nitromethane fuel. High-speed taxi tests (Figure 28) quickly revealed that the ailerons had to be set on the HIGH setting of the transmitter for sufficient lateral authority in the 2-1/2 to 4 knot crosswind component to keep the upwind wing down. Additionally, the aircraft was especially sensitive to NWS inputs, even on the LOW setting. However, the pilot quickly grew accustomed to the NWS sensitivity.

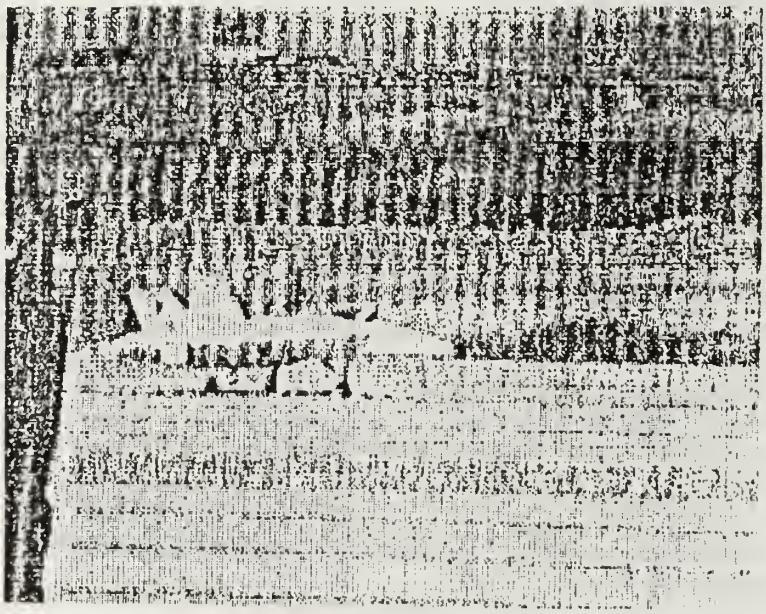

Figure 28 High-speed taxi testing.

The first flight began with a flaps-up takeoff, with the landing gear remaining in the down position. Acceleration was brisk, with the estimation of 21 to 22 lbs static installed thrust made in section C.7.b a reasonable guess. Rotation was smooth and the takeoff roll was estimated to be 100 to 150 feet.

The model climbed out steeply, and the pilot commented that it was very controllable. Four passes were made overhead the runway, with the third pass being trimmed up and hands-off by the pilot (Figure 29). The fourth pass featured full-deflection aileron rolls in both directions, with rather sluggish response (aileron controls were on the HIGH setting). With the throttles at full power, the estimated level maximum airspeed was approximately 80 to 90 mph.

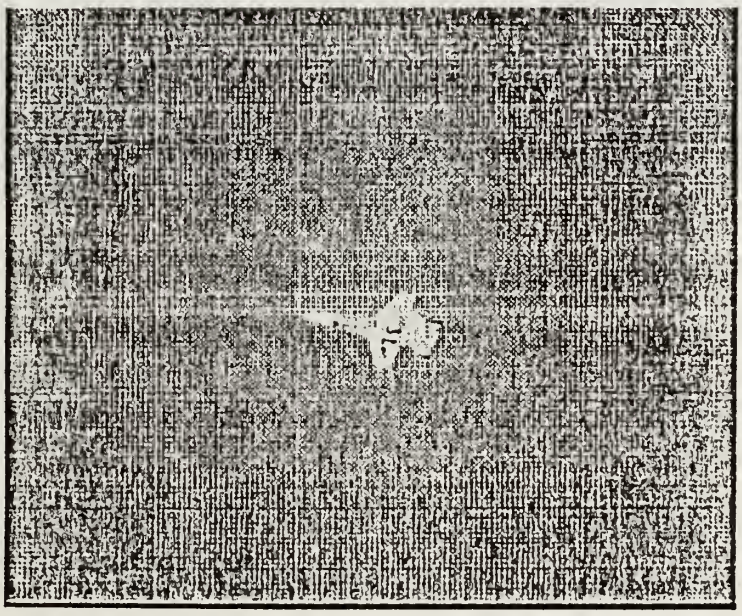

Figure 29 Hands-off trimmed flight on third pass over the runway.

As the pilot began the final turn to the runway from the downwind leg, he noticed little apparent response from the engines when he attempted to throttle back. He announced the problem and continued to modulate the throttle joystick in an attempt to regain control of the engines. The engine(s) modulation could clearly be heard. At about the 135° position in the approach turn, the engine noise abruptly changed and stayed steady, and it immediately became apparent that the model was then single-engine, with no control over the power. The model flew very high overhead and landed well down the runway, approximately 300 to 500 feet from the pilot and observers. The pilot flared too high, and the aircraft picked up a substantial right drift just prior to landing very hard. The right main landing gear was broken off at the trunnion bolt and the model slid to a stop, the single engine still running at about 1/3 power.

After the right engine was manually shut down, inspection revealed little damage to the model's underside. Apart from the sheared landing gear trunnion bolt, which has since been easily repaired, the right wingtip sustained some minor abrasion damage. The cause of the stuck throttle condition was the right carburetor barrel slot guide screw, which had vibrated loose about 1-1/2 turns and jammed the carburetor barrel. Likely, the other engine quit during the rapid throttle modulations as the pilot was attempting to ascertain the reason for the lack of power response. Ducted-fan engines can be susceptible to quitting during many rapid and large throttle excursions, choking and flooding from the large mixture changes that result.

Additionally, and potentially very serious, the right engine exhaust pipe had fractured approximately 3-1/8 inches aft of the forward flange (Figure 30). This left the aft part of the pipe dangling from its connection to the fuel

pressurization line. Although the possibility is remote, this broken pipe could have come loose and slid aft to the elevator control shaft, with the potential of jamming the elevator. Or the pipe could have simply fallen out of the tailpipe duct, posing a hazard to people on the ground.

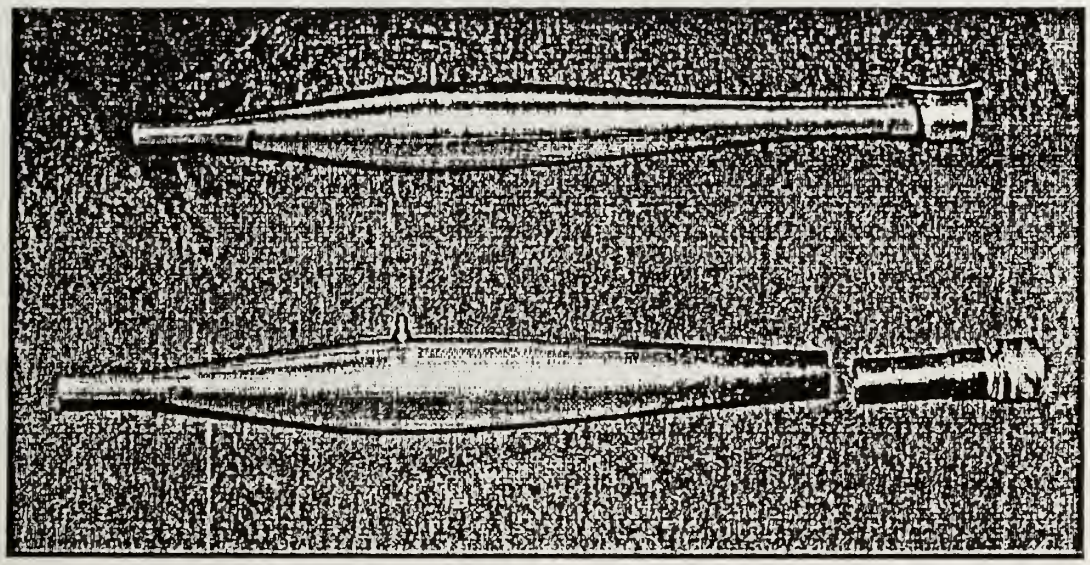

Figure 30 Comparison of intact and broken exhaust pipes after first flight.

Inspection revealed that the rubber exhaust O-ring appeared to have burned away completely. Whether it was gone prior to the fracture or afterwards cannot be determined, but Mr. Callaway stated from experience that the loss of the O-ring likely caused severe vibration between the exhaust

manifold and the mounting flange of the pipe, causing it to crack and eventually break.

2. Recommendations

Future flights should be with wind no greater than 5 knots, with a crosswind component no greater than 2 knots. If the parachute had been needed on the first flight, it is certain that major drag damage would have resulted.

All engine-critical fasteners, such as the carburetor barrel slot guide screw, need to be secured with Loctite. Better-quality exhaust O-rings have been obtained, and should be inspected after each flight and replaced if there is any visible damage, such as tearing or signs of exhaust blow-by or burns. The particular exhaust tuned pipes used were designed for the OS-77 engine. Jet Model Products, Inc., markets a tuned pipe designed for the OS-91 engine, which should be used in the future. This pipe is longer in length with a slightly larger exit diameter.

Prior to the next flight, the maximum installed static thrust should be determined. This can easily be accomplished at the UAV Lab.

IV. F/A-18 UAV FUTURE OBJECTIVES

When the F/A-18 UAV enters the next phase of the flight test program, with proper instrumentation installed, stability and control derivatives can then be determined. Following that, the high-AOA supermaneuverability research can commence. The UAV aerodynamics researcher should ask the following questions: What is the quantitative information being sought? What about scaling factors? What about Reynolds number effects? Is vortical flow extra-sensitive to Reynolds number? Does one have a basis for good qualitative judgement of the observed responses to the controls inputs?

Specifically, one desires to know what to expect a generic fighter UAV to achieve in supermaneuverability and agility in angle-of-attack areas that severely limit the performance of current fighter aircraft and that will require the design and implementation of non-conventional flight controls. The matching of Reynolds number for equivalent airflow and performance parameters is very difficult for small-scale models [Ref. 28]. Scaling factors are available that can lend considerable insight and help predict dynamic behavior, even if the small-scale UAV, such as the 1/7-scale F/A-18, is not accurately dynamically-scaled.

A. THE HIGH AOA, POST-STALL PROBLEM

1. High AOA Characteristics

An imperative performance parameter for agile fighter aircraft is good behavior in the high AOA, post-stall phases of flight. What is "good behavior"? Certainly, reliable engine performance is required. The pilot cannot engage in tight, dynamic maneuvering with fear and trepidation of throttle and afterburner

transients in an arena that will certainly see large negative and positive G and AOA excursions. Also, cockpit ergonomics and human factors engineering play an equally important role.

And what of the stability during steady-state maneuvering and agility during dynamic maneuvering of the airframe? There is little advantage in having an aircraft with tremendous pitch authority to pulse to very high angles of attack, only to be so directionally unstable that the pilot cannot perform a tracking solution, or worse yet, loses control. Either of these could be fatal in air combat. Likewise, a tactical aircraft must also demonstrate satisfactory agility and control while maneuvering with reasonable asymmetric stores loading configurations and while passing through normally unstable AOA thresholds that present severe control problems. With digital flight control systems, the software engineer can write the proper control laws that use active flight controls to compensate for asymmetric stores, unusual and unstable transient thresholds and high-AOA directional instability. However, high-AOA directional instability still requires physical aerodynamic devices to control the yaw authority problem depicted in Figure 1 of Chapter I.

2. The Directional Stability Problem

Although there is little tactical value in flying at extreme angles of attack, the fighter pilot often finds himself there in spite of the tactical dangers, and he must be comfortable there with both his skills and the aircraft. Current aircraft, such as the F-14, F/A-18, F-15, and F-16, generally exhibit good high AOA behavior. But any aircraft will eventually depart controlled flight when pressed beyond its limits, with the potential for loss of control. Despite sophisticated software control laws in current state of the art fly-by-wire (FBW)

flight control systems, physical aerodynamic devices are still required to provide adequate control at "the edge" when the conventional controls no longer work.

As the AOA gets very large, the vertical tails become immersed in low-energy air that reduce their effectiveness [Ref. 2]. The blanketing effect on the vertical tail(s) by the stalled wake of the wing leads to the suggestion that large improvements in the effectiveness of the conventional rudder may not be obtainable [Ref. 2]. Knowing that the high-AOA characteristics of fighter aircraft can be highly configuration dependent, the evaluation of yaw control devices such as strakes takes on great research significance.

Recall from Figure 1 that once the AOA passes the intersection of rudder power available with rudder power required, there is little perturbation needed to start the aircraft yawing uncontrollably toward a departure. The highly dynamic combination of high-AOA flight and ACM will certainly see to that. Thus we have the root cause of departures: an uncontrollable yaw, almost always coupled with roll and/or pitch excursions, that temporarily render the pilot a passenger in his own machine. As a rule of thumb, the higher the AOA at onset of the departure, and the higher the already established values of yaw and roll rates, the more prolonged and violent the departure will likely be. The only current cure to regain directional stability is to retain sufficient pitch authority (or possess perhaps a great deal of fortune or a spin chute) to move the nose back down into a fully-flyable angle-of-attack region.

B. CONTEMPORARY RESEARCH IN NON-CONVENTIONAL YAW CONTROL

References 2 through 5 describe detailed investigations that use the non-conventional methods of forebody strakes and pneumatic blowing. The

preferred method for this author is the use of strakes. At high AOA, vorticity is generated on each side along the length of the forebody. The idea is to manipulate the strong pair of vortices that are generated at the tip of the nose and trail behind on each side of the forebody in a similar manner to streamers in the wind attached to the top of a pole. At lower AOA's, the vortices are relatively weak, but can still produce yawing moments if asymmetrically deflected with strakes. At AOA's beyond approximately 25° to 30°, the vortex pair becomes increasingly stronger, just as the vortex pair does from the forward edge of the LEX's [Ref. 22]. The investigations of References 2 through 4 are especially detailed in the design and size of the strakes, and the resulting yaw moments at high AOA's generated by the asymmetric deployment of the strakes ($C_{n_{strake}}$) are generally stronger than those generated by the rudders at lower AOA's.

1. Forebody Vortex Description

Figure 31 [Ref. 3:p. 4] clearly shows a frontal view of how the vortex pair forms on each side of the forebody. With symmetric strakes (or no strakes), the vortex pair is generally symmetric. With the asymmetric deflection of a strake, the two vortices are no longer a mirror image of each other. Generally, if a vortex is forced sufficiently away from the forebody while the other one remains undisturbed, the pressure distribution around the forebody is asymmetrically affected, generating a side force on the forebody. The side of the deflected vortex experiences an overall increase in pressure distribution, caused by the spoiler action of the strake. This produces separated and increased-turbulence flow with a region of pressure that increases rapidly to near that of ambient. The other side still has relatively smooth, attached flow with a

low pressure distribution. Bernoulli's law applies here now, just as on a wing, and side "lift" is generated.

References 2 through 4 reveal that significant yawing moments are generated at high AOA's with the use of strakes, generally over twice that provided by the rudder(s) at low AOA's. Essentially, the F/A-18 and generic fighter models studied had suffered total loss of rudder authority beyond about 65°, while the aircraft became increasingly unstable in yaw. The direction of the yawing moment is highly sensitive to both the radial orientation of the strake pair and the deployed height of each strake.

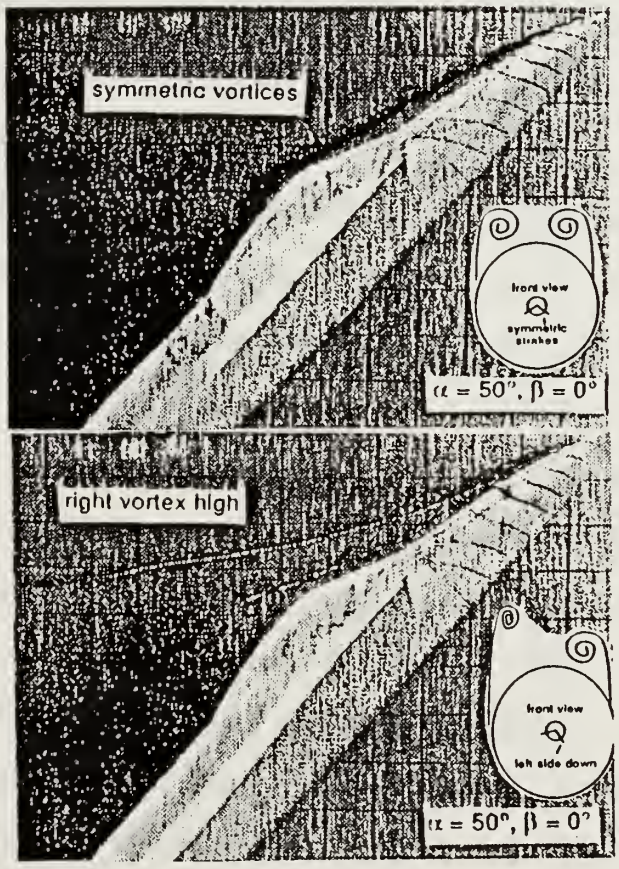

Figure 31 Forebody vortex pair [Ref. 3].

2. Location of the strakes

Investigation has concluded that a ± 105° orientation from the windward meridian is the best radial location for the strake pair. The windward meridian is the imaginary line drawn from the tip of the nose along the bottom of the radome that is facing the relative wind. The lee meridian would be 180° away, along the top of the radome. Malcolm et al. [Ref. 4] found it was desirable to mount the strakes as far forward on the nose as mechanically possible. Both Malcolm et al., and Murri and Rao [Ref. 2] experimentally arrived at the aforementioned ±105° radial orientation of the strake pair as the best location. Figure 9 of Reference 2 clearly illustrates this, with consistent, smooth and predictable changes of $C_{n_{strake}}$ with angle of attack.

Several variations on the actual construction of the strakes were investigated in References 2 through 4, including fixed strakes mounted on a rotating nose cone cap (Figure 32), clamshell-type strakes that open and shut like doors, and the forward pivoting type that translate in and out of the forebody in the same manner as the glove vanes do on the F-14 (Figure 33). The simplest design appears to be the latter.

3. Height of the Strakes

In the case of the translating-type strake, the angular displacement also is a significant factor in the effect the strake has on the yawing moment. In Reference 4, this is referred to as strake height, i.e., how far out the strake is deployed from its flush, non-deployed position. Interestingly, if the strake is deployed only a small amount, the yawing moment is into the direction of the side of the deployed strake (right strake deployed, nose yaws right).

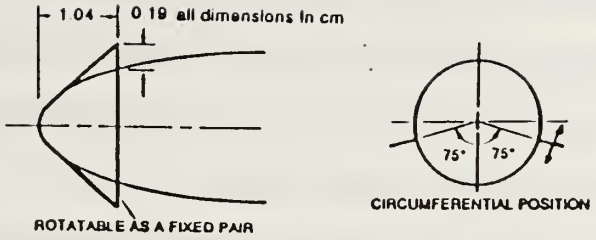

Figure 32 Rotatable forebody strakes [Ref. 3].

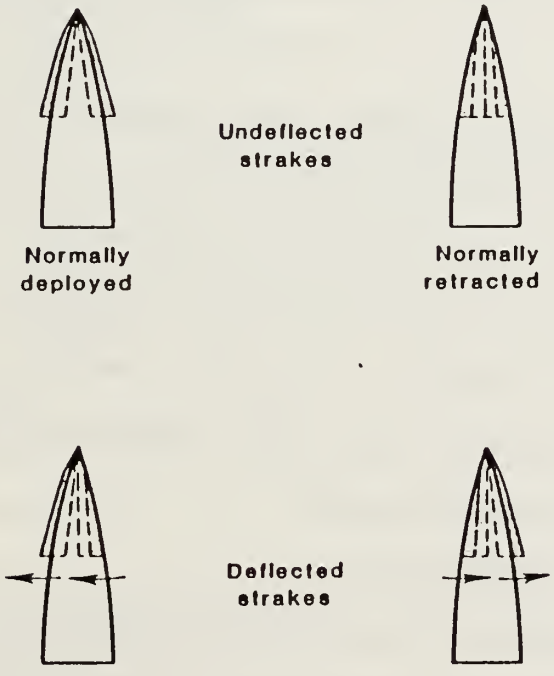

Figure 33 Pivoting-type, translating strakes [Ref. 2].

However, if the strake is further deployed beyond a certain threshold height, the yaw moment is reversed, and the nose yaws in a direction away from the side of the deployed strake. This phenomenon was alluded to earlier in section B.1. Malcolm et al. in Reference 4 experienced this very unexpected result while evaluating variable strake heights.

For clarity, their strake height was referenced to the forebody diameter d. The strake pair was 1.0d in length, and deployable to a height of .08d. They discovered that when the translating-type strake was deployed approximately halfway (.04d), the model yawing moment was toward the same side. As the strake was deployed further, the yawing moment trend reversed and shifted to the other direction, becoming negative (away from the side of the deployed strake). They explain this by suggesting that an insufficient height of the strake was not enough to keep the displaced vortex airflow detached, and it soon reattached, with an actual stronger negative pressure gradient, and thus stronger suction, on that side than the other side's "clean", still attached vortex flow. One may conclude from this that to avoid this odd, ambiguous region of reversible yawing moment, the strake should be clearly deployed to a robust height to ensure a positive separation of the vortex that has no chance to reattach. Incidentally, Reference 4 did not include a discussion of Reynolds number effects transferable to full-scale aircraft tests.

4. LEX Coupling Effects

Murri and Rao of Reference 2 discovered that as sideslip angles were generated at high AOA in conjunction with strake deployment, there was a strong coupling with the LEX vortex flowfields that produced a significant rolling moment, which was proverse in nature. Smoke flow visualization tests

revealed that the very powerful LEX vortices experienced asymmetric bursting that produced the rolling moments. Shah in Reference 22 revealed that the LEX vortices are responsible for 30 percent of the total lift at $C_{L_{max}}$. This is not merely from the additional wing area the LEX's offer, but from the powerful suction caused by the strong vortex cores. Thus, it is easy to see that any modification to the forebody vortex field is going to affect rolling moments with any application of sideslip. Shah also tested variations in LEX chord and span, and the effects of the vortex fence that is mounted on the LEX of all current F/A-18's, which was designed to alleviate vortex burst-induced buffeting and resulting structural fatigue of the vertical tails. The LEX fences slightly dilute the vortex cores' strength, while moving them slightly outboard of the tails.

C. MODEL SCALING FACTORS

1. Thrust and Weight

Hall of Reference 28 explains that similarities between a scaled model and the full-scale aircraft can only be relied upon if the model is accurately dynamically scaled to reflect similar observations, such as moments of inertia, pitch/roll/yaw rates, and so forth. The model should be as large as practicable in order to hold the weight to scale values, and to reduce the uncertainty of Reynolds number effects. The scale of the model is denoted by λ. The F/A-18 UAV is a 1/7-scale model; thus λ is 7. However, not all is so simple. The aircraft may be 1/7th the length, height, and so on, but weight, volume, moments of inertia, and many other performance factors vary as some power of λ. Some representative scale factors are shown in Table 6 [Ref. 28].

For example, since volume is $lxwxh$, then the model will have $1/\lambda^3$ the volume of the full-scale aircraft. In this case, the F/A-18 UAV has 1/343th

(0.0029) the volume of the actual aircraft. Weight varies also as the cube of the scale factor. If the 1/7-scale F/A-18 were to be accurately scaled to reflect a clean-configured F/A-18C, weighing 35,300 lbs with full internal fuel and no Sidewinder rails, the model would need to weigh approximately 103 lbs, which is about 3.25 times more than the current fully-fueled weight of 31.55 lbs.

TABLE 6

Model Scale Factors

Parameter	Model should be:
Linear dimension	Full scale/λ
Area	Full scale/λ^2
Volume, Mass, Force	Full scale/λ^3
Moments	Full scale/λ^4
Moments of Inertia	Full scale/λ^5
Linear velocity	Full scale/$\lambda^{1/2}$
Linear Acceleration	Full scale/$\lambda^{1/2}$
Angular acceleration	Full scale $\times \lambda$
Angular velocity	Full scale $\times \lambda^{1/2}$
Time	Full scale/$\lambda^{1/2}$
Work	Full scale/λ^4
Power	Full scale/$\lambda^{5/2}$
Wing loading	Full scale/λ
Power loading	Full scale $\times \lambda^{1/2}$
Angles	Full scale $\times \lambda^{1/2}$

The full-scale aircraft has a near 1:1 thrust/weight ratio (T/W) on takeoff (about 0.91), yet the current T/W of the F/A-18 model is only 0.7, based on an estimated 21.5 lbs maximum available thrust. Currently, there are no existing engines small enough that provide the required T/W of 1:1 for the current model configuration, and certainly none are available to provide 1:1 for a scaled weight of 103 lbs. Additionally, the model would require quite extensive structural modifications to bear the extra power and weight stresses.

It would be important to have T/W near that of full scale to keep the model's performance similar when it flies in very high-AOA, steady-state maneuvers. Otherwise, low T/W values will result in high sink-rate conditions that will increase the difficulty of the UAV pilot to fly precise test parameters and limit data collection time.

2. Reynolds Number

One of the main difficulties of relating model testing to full scale is the effect of Reynolds number (R_e). Reynolds number can be calculated from Equations 10 and 11. Reynolds number is a similarity parameter that reflects the strength of inertia forces relative to viscous forces in the flow [Ref. 29]. Hall of Reference 28 explains that so long as the Reynolds number stays above approximately 120,000, the more accurate the extension of model flight data to full-scale. In the case of the several forebody strake investigations cited in this report so far, typical Reynolds numbers based on the forebody base diameter, d, have been in the range of 109,000 to 200,000. Murri and Rao [Ref. 2] stated that even though their Reynolds numbers were low, the effects on forebodies are generally minimized when the flow separation is fixed with strakes, and thus their tests were considered valid assessments of the actuated strake concept.

Thus, the data generated may be applicable to the full-scale aircraft. Calculations for the F/A-18 UAV will be presented later.

3. Other Scaling Problems

To illustrate further the difficulty of scaling a flying model that is representative of a modern high-performance jet, data comparisons are presented from Tables 4 and 5 in Chapter III. If the F/A-18 UAV data were to be scaled upward from its present gear-retracted I_{xx} value of 0.281 lb-ft-sec^2, it would be 4722.8 lb-ft-sec^2. Similarly, the values for I_{yy} and I_{zz} would scale up to 29,849 and 31,296 lb-ft-sec^2, respectively. Since these values fall into a range 20 to 22 percent of full-scale, they may present useful numbers when used with correction factors. For example, since angular acceleration of the model should be full-scale times the model scaling factor (Table 6, "Angular Acceleration"), then one may assume that the model's yaw rate acceleration ($\dot{r}$) due to $C_{n_{strake}}$ might be approximately five times that of the correctly scaled model.

The scaled-upward value for weight would be 10,804 lbs, which is a little less than a third of full-scale. Scaled-upward thrust is approximately 22 percent that of full-scale at 7200 lbs. In brief summary, the F/A-18 UAV scaled-upward numbers, using the parameters of Table 6, fall into the 20 to 32 percent area of full-scale. The only unrealistic scale comparison is top speed. The full-scale aircraft obviously operates in the compressible flow region and into supersonic airspeeds. Its top speed at sea level of 725 KCAS/1.1 Mach is very likely a Q limit based on structural and aerodynamic heating considerations. So there is little value in comparing the model's scaled-upward estimated top speed of approximately 350 knots, a limit based on available power.

Yet, there are some useful observations to study further. In Chapter III, it was noted that the gear-retracted Roll/Pitch Inertia Ratios I_{xx}/I_{yy} were very similar. The full-scale F/A-18 has demonstrated instability in the longitudinal axis (inertial pitch coupling) when doing multiple aileron rolls, which manifests itself in violent departures in the worst cases [Ref. 25:p. 4-2]. It can happen during any high roll/yaw-rate roll, but is more noticeable when rolling at AOA's above 20°. The yaw rate must be actively and aggressively controlled. Coordinated rudder actually exacerbates the problem. Additionally, rolling at less than 1 G (i.e., a normal aileron roll) can cause the aircraft to diverge because of large roll-coupling tendencies; zero G is worse than 1 G [Ref. 25:p. 4-2]. After the departure occurs, the AOA and yaw rate combination can progress to the point where forward stick to counter the increasing AOA will not overcome the more powerful inertial forces. Thus, the roll rate must be stopped as soon as the pilot sees the AOA start to diverge.

Any aircraft that has a similar low inertia ratio, which happens to include virtually all tactical jet aircraft, may be prone to have this kind of instability. This can be seen from Equations 12 and 13 [Ref. 30], where I_{xx} is much smaller than either I_{yy} or I_{zz}. Careful examination of the rolling moments equation also reveals that if the product of inertia about the xz axis (I_{xz}) is non-zero, then it influences the aircraft in pitch. When I_{xz} is non-zero, whether negative or positive, it means that the principle momentum axes are not aligned with the aircraft reference axes. The computation of I_{xz} is determined by the second triple integral in the top row of Equation 13. The influence of I_{xz} in all the relations of Equation 12, in conjunction with the value of I_{xx} being much smaller than both I_{yy} and I_{zz}, means that the aircraft, when rolled rapidly, will

tend to couple in pitch and roll, seen as the nose beginning to cone around the roll axis on the horizon, and can diverge to the point of departure from controlled flight if not attended to (see previous paragraph). This coning is the aircraft's AOA diverging as it rotates around its principle momentum axis vice its roll axis.

With that said, there are not enough flight data yet to support the notion that the F/A-18 UAV will exhibit a similar tendency for pitch-roll coupling during high roll rates, because the value of I_{xz} has not been determined for the model. However, if future flight test requirements dictate the need to explore high roll rates, the model needs to be closely monitored for any tendency of pitch-roll coupling.

D. ESTIMATED MODEL AERODYNAMIC CHARACTERISTICS AND PERFORMANCE

1. Estimation of Maximum Speed and C_{D_0}

Parker [Ref. 31] estimated the full range of performance parameters for a UAV designed to be similar to the Pioneer UAV. His well-executed treatise and detail of the subject for this application is beyond the scope of this investigation. However, some performance parameters may be estimated through simple calculations with a reasonable degree of confidence.

Equations 14 through 18 were used to arrive at a value of C_D, and through an iteration process of feeding back computed values of maximum speed and recalculation of the drag coefficient, reasonable values for v_{max} and C_{D_0} were determined. With the aforementioned equations, the following assumptions were made:

Oswald Efficiency Factor -	$e = 0.6$
Fan Efficiency -	$\eta = 0.85$ to 0.90
Maximum thrust -	$T_{max} = 20.25$ to 21.5 lbs
	(assume flat thrust curve)

Equation 14 is manipulated into Equation 15, assuming the engines are at full power and thus producing full available thrust. The engines produce 4.8 BHP each, and the flat thrust curve assumption is based on the jet-like propulsion system of the ducted fan design. No information is available for fan efficiency, so a range of 0.85 to 0.90 was assumed as a best guess. When the range of assumed thrust and fan efficiency parameters are substituted into Equation 15, a v_{max} range of 208.7 to 234.7 ft/sec (142.3 to 160 mph) was determined. Mr. Callaway had estimated the F/A-18's top speed would be in the 130 to 150 mph range, so these results were a good ballpark start. The reader will recall from Chapter III that the estimated level-flight maximum speed on the model's first flight was 80 to 90 mph (gear down).

Next, a cross check of a reasonable determination of v_{max} using Equation 16 was conducted. This equation requires the additional assumption of some initial value of C_{D_0} to determine v_{max}. The reader will note this is a simple fourth order relation that may be easily iterated upon or solved by use of a quadratic reduction formula. Guesses of 0.032 and 0.042 were used to arrive at a calculated speed range of 209.7 to 248.1 ft/sec (143 to 169 mph). The high value of 169 mph came from a thrust of 21.5 lbs and C_{D_0} of 0.032, and is not a reasonable value. Equation 19, the jet thrust equation [Ref. 32], states that the freestream velocity of the aircraft cannot exceed the exhaust velocity. The

brochure material for the Dynamax Ducted Fan Units claim a maximum exhaust velocity of approximately 170 mph using OS-77 engines. The maximum exhaust velocity with OS-91 engines was not available, but likely is not much higher. Thus, a v_{max} of 169 mph is highly unlikely in level flight. The full range of calculations are found in Table 7.

TABLE 7

Speed and Drag Coefficient Range Iterations

Parameters	Maximum speed
η=.85 to .9, T=20.25 lbs	v=221.6 to 234.7 ft/sec
η=.85 to .9, T=21.5 lbs	v=208.7 to 221.0 ft/sec
C_{D_0}=.032, T=20.25 to 21.5 lbs	v=240.6 to 248.1 ft/sec
C_{D_0}=.042, T=20.25 to 21.5 lbs	v=209.7 to 216.2 ft/sec
Thrust and speed values	Drag Coefficient
T=20.25 lbs, v=221.6 ft/sec	0.0382
v=234.7 ft/sec	0.0340
v=240.6 ft/sec	0.0324
v=209.7 ft/sec	0.0426
T=21.5 lbs, v=208.7 ft/sec	0.0430
v=221.0 ft/sec	0.0384
v=248.1 ft/sec	0.0305
v=216.2 ft/sec	0.0401

After the initial round of calculations were completed, average values of v_{max} and C_D were selected and cross checked with each other. Final results of 225.9 ft/sec (154 mph) for v_{max} and 0.0370 for C_D were determined. Next, using Equation 17, the maximum-speed value of C_{D_i} was calculated to be

$4.74X10^{-4}$. From this, the final value of C_{D_0} of 0.0365 was obtained. These values for maximum speed and zero-lift drag coefficient appear to be reasonable for a 1/7-scale model.

2. Lift Slope and Maximum Coefficient of Lift

Examination of the F/A-18 UAV's wing and careful comparison with the airfoil shapes in Reference 33 indicate a close resemblance to the NACA 64-209 airfoil. This airfoil has a lift-curve slope a_o of 0.1074 per degree, close to the theoretical ideal value of 0.110 per degree dictated by lifting line-theory. The ac ranges from 0.258 to 0.261, and the airfoil has a no-flap $C_{l_{max}}$ of 1.2, with a very sharp break at the peak. With a 0.2c split flap extended to 60°, $C_{l_{max}}$ increases to approximately 1.95. Stall occurs at about 13° AOA for no-flap and about 7° AOA for flaps down.

Aspect ratio and 3-D corrections will lower the lift-curve slope and result in a no-flap stall at higher AOA's, although at a lower value of $C_{L_{max}}$. This is illustrated in Figure 34. Recalling the aspect ratio of 3.532 for the model, and the assumption of 0.6 for e, Equation 20 is used to determine the new, effective lift slope of the F/A-18 UAV's wing. Typically, e for most aircraft falls in the range of 0.7 to 0.85. However, there are exceptions. Recent flight testing of a Merlin III twin turboprop general aviation aircraft revealed an Oswald efficiency of only 0.5, even though it had a relatively high AR of 7.71 [Ref. 34]. As a general rule, as AR decreases, so does e, along with the lift-curve slope [Ref. 35]. Since the F/A-18 has a small aspect ratio, along with lower efficiencies associated with large leading edge extensions, a guess of 0.6 for the Oswald efficiency factor is justified. When the model is later instrumented and

performance data can be obtained, a plot of C_D versus C_L^2 will allow e to be determined, as shown in Figure 35.

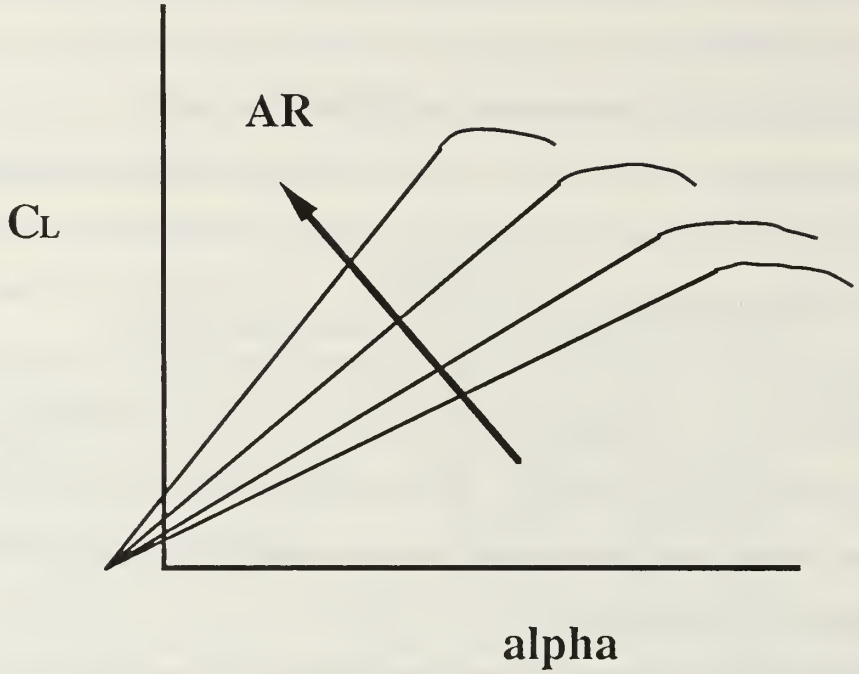

Figure 34 Plot of lift-curve slope as a function of AR [Ref. 35].

With an airfoil lift-curve slope a_o of 0.1074, e of 0.6 and AR of 3.532, Equation 20 yields an effective lift slope of the wing a_w of 0.0558 per degree (3.197 /rad). With an assumption that the wing now stalls at an AOA of approximately 18°, then $C_{L_{max}}$ would be approximately 1.004 for a no-flap, no-leading-edge-device wing. If the same 62 percent increase in lift from flap deflection is available, then a full-flap $C_{L_{max}}$ of approximately 1.62 could be expected. Using Equation 21, a no-flap, power-off stall speed, using 1.004 for $C_{L_{max}}$, standard sea level density and a weight of 31 lbs, calculates to be about 36 mph, which appears to be reasonable. Wing chord Reynolds number would be about 600,000 at this speed, and 140,000 for the forebody. Reference 22 obtained values of $C_{L_{max}}$ (LEX removed) of about 1.2, although at a much

higher R_e than would be encountered in 1 G flight. However, the data for the 16 percent scale F/A-18 of Reference 22 were obtained with leading edge flaps set at 34°. The F/A-18 UAV currently has no leading edge flaps, which will require major modification or procurement of another wing set to make the modification. Reference 22 shows that the LEX's account for 30 percent of the lift at $C_{L_{max}}$, so the model can reasonably be expected to stall at a lower airspeed/higher AOA.

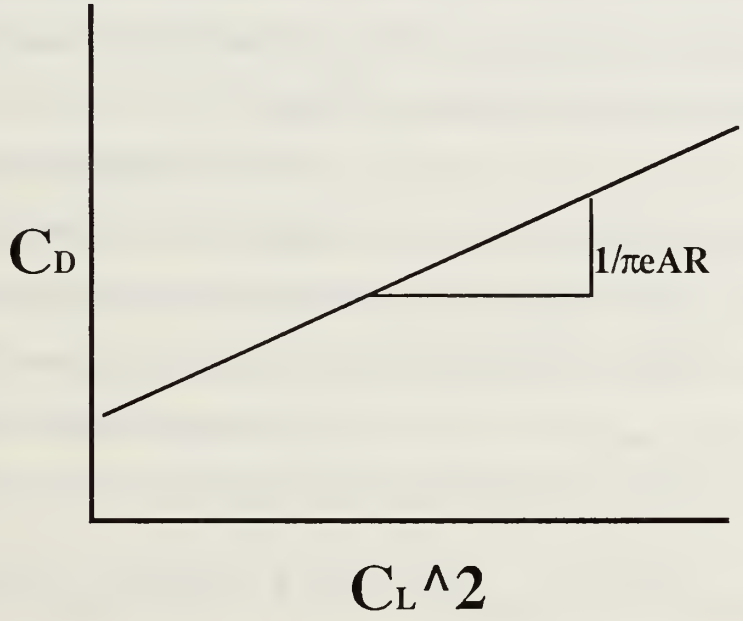

Figure 35 Determination of e.

3. Estimation of Stick-Fixed Neutral Point and Static Margin

The horizontal tail is symmetric. From past experience in evaluating neutral points, the lift slope of the tail is generally less than that of the wing, with the ratio a_t/a_w typically 0.75 to 0.85. In evaluating the location of the neutral point, the change of horizontal tail downwash from the wing with change in

AOA was determined. Using Equation 22 [Ref. 31], with a m.a.c. of 20.65 inches and l of 30.89 inches, $\partial\varepsilon/\partial\alpha$ was determined to be 0.322. Next, Equation 23 was used, with the assumption that the influence of the LEX's would move h_{ac} forward from the average value of 26% m.a.c. to a conservative estimate of 22%. When the appropriate values were substituted into the equation, using a tail-to-wing slope ratio (a_t/a_w) of 0.80, h_n was determined to be 39.2%. With the current cg at approximately 16%, this yields a static margin of approximately 23.2%. Since the full-scale F/A-18 generally encounters longitudinal control and stability problems with the cg aft of 25% m.a.c. [Ref. 25], it is recommended that future research be confined to the same aft limits.

The stick-free neutral point (h_n') cannot be determined because of the nature of the servo control system on the flight controls, which act in a similar manner to irreversible flight controls. There is no such thing as "hands off, stick-free" in the classic sense of that of a conventional, unpowered flight control system. As aerodynamic forces try to deflect a surface from its commanded position, opposite servo forces drive the control surface back to its null position.

E. FUTURE RESEARCH AND DESIGN MODIFICATIONS

1. Forebody Modifications

Examination of References 2 through 4 indicate that the use of strakes would be preferable over the use of pneumatic control methods of Reference 5. As a practical matter, the strakes would likely be easier to install than a pneumatic system. Advantages include using an already available power supply for strictly electrical control, and the ability of vernier control. A pneumatic system would require a consumable air supply that may limit flight time, and

would need some way of precise vernier air control to explore the subtleties of variable flow rates.

Strakes might easily be implemented by making the radome detachable to allow easy access to the forebody, and to allow relatively quick modifications. As an initial baseline strake design, the recommendation is to use a ± 105° orientation for the strakes, translating in and out from a forward pivot point. This design would most likely allow viable results from the first flight test, and the pivoting design would allow a smooth, flush exterior. The only drawback is the room required inside the radome to accommodate the stakes when they are stowed. An additional receiver will be required to power the possible extra two servos, one for each strake.

As mentioned in the previous section, at the low-speed, high AOA regime near the stall, the forebody Reynolds number would be about 140,000, which would be comparable to those of References 2 through 4.

2. Wing Modifications

Personal F-14 flight experience indicates the F/A-18 UAV will very likely encounter lateral instability in the form of wing rock when subjected to very high AOA flight, made worse by the absence of leading edge flaps. The full-scale F/A-18 does not experience wing rock as severe as that of the F-14 because of the nature of the LE flaps design and the excellent execution of the FCS software. Leading edge flaps (slats) attenuate this instability and increase the maximum coefficient of lift at a higher AOA. It is recommended that the wings be modified or replaced with properly configured wings as soon as practicable as a step toward the high-AOA flight research using forebody strakes. No information is available whether the installation of the Sidewinder

rails would improve lateral stability, but their use would complicate the location of an airspeed system.

3. Instrumentation of the F/A-18 UAV

Once the F/A-18 UAV flight controls are instrumented and the airspeed, AOA and sideslip transducers are installed, control and stability derivatives (C_{M_α}, C_{M_q}, C_{n_β}, C_{M_0}, C_{l_β}, C_{y_β}, $C_{M_{\delta_e}}$, $C_{l_{\delta_a}}$, and $C_{n_{\delta_r}}$) can be determined. The telemetry system that was developed and flown on the testbed F-16 UAV has been calibrated and verified in flight, with consistent data downlink to the ground recorder [Ref. 36]. The telemetry system also recently flew on the UAV Lab's 1/2-scale Pioneer, with satisfactory operation. With the telemetry system installed on the F/A-18 UAV, for example, one can accurately determine the stick-fixed neutral point by plotting the data of $d\delta_e/dC_L$ versus cg [Ref. 35:p. 4.9].

4. Fly-by-Wire Flight Control System

An excellent thesis topic would be a cooperative effort with the Department of Electrical and Computer Engineering to design, construct and install a digital flight control system (DFCS) to achieve active flight controls for the F/A-18 UAV. A suggestion to save weight would be to implement a hardware design that would connect a laptop 386/486 or Macintosh-type computer via digital to analog (D/A) interface to a computer "module" on the ground. The module would be driven by the software in the laptop computer that contain the control laws to operate the flight controls, essentially being the DFCS computer on the ground vice in the aircraft. This could be accommodated by installing another receiver in the aircraft to achieve fully independent articulation of all the flight controls. Each channel of the receiver would

correspond to the appropriate channel driver of the module. The normal hand-held Futaba 1024A transmitter signals would go through the module. In the event of a DFCS malfunction, the system would be switched back to a normal fail-safe standard configuration, with the Futaba 1024A transmitter linked directly to one of the aircraft receivers. Presently, the rudders are both on one channel, as are the ailerons and the horizontal tails. The ailerons already have their own individual servos, but the rudders and horizontal tails each would need another. In addition, the horizontal tail would need to be structurally modified to be made into two independent surfaces. For simplicity, the leading edge flaps modification should be made ground-adjustable only, unless future research plans dictate the need to modulate them while airborne. The major obstacle to this modification plan is the additional weight, which would include at least two servos (in addition to the two servos needed for the forebody strake modification). The model is already heavy, and the instrumentation, extra wiring, connectors, servos, extra capacity power supply, telemetry system and so forth may easily increase the weight another three to six pounds. Since receivers are only 1.3 ounces, it seems logical to keep as much of the computer hardware on the ground as possible in the event DFCS becomes a research requirement in the future.

V. RESULTS AND CONCLUSIONS

The F/A-18 generic fighter UAV has been completed and successfully flown. Future high-angle-of-attack research needs more aggressive funding to explore the high-risk flight regimes for which the model is designed. The lessons learned and valuable flight data will hopefully reduce the inadvertent loss of manned aircraft and improve high-AOA controllability in the future.

The parachute recovery system was modified mostly in the execution and design areas from the original plans of Reference 18, but not in the basic concept of operation. Prudent and well-planned flight testing should not result in its use, but it is there just in case to help preserve the tremendous amount of investment in the aircraft.

More funding and a greatly-streamlined acquisition process is needed to procure spares, fuel and other equipment to keep the program moving. Out-of-pocket expenses just to keep the program from stagnating will become too much of a financial burden simply because of the cost of some of the high-ticket hardware such as receivers, potentiometers and gearing, servos and other model-peculiar items. The correct tuned exhaust pipes need to be ordered (almost $100.00 each), and the exhaust O-rings need the utmost attention in flight operations. At around four to five dollars per O-ring, this becomes an expensive consumable item.

The aircraft has adequate internal room to move components around to investigate the effects of various cg locations. Although the model presently has plenty of room for additional equipment, weight growth must be carefully monitored. Only a few more pounds will drive the T/W toward 1:2, and the

high AOA supermaneuverability research would be severely hampered. With this in mind, since it is almost impossible to have too much power in any fighter, generic or real, more powerful engines should be sought. With induced drag surely to be a very significant factor when the model is in the post-stall flight regime, the high AOA research would benefit greatly if the total installed thrust could be increased to at least 28 to 30 lbs.

A flight proficiency program needs to be implemented to keep the F/A-18 UAV pilot's skills sharp in order to fly maneuvers accurately and very precisely, which will be imperative in the supermaneuverability research. A recommendation is to conduct F/A-18 UAV flight operations at least twice monthly, with two to four sorties for each training session. Funding needs to be established for this training. It is this author's opinion that quality flight time and proficiency will indeed be needed to attain the precision needed to fly the high-AOA maneuvers required for consistent high-quality data acquisition. The high-AOA research should always be conducted in still air if practicable.

Joint thesis studies, in particular involving the design, development and installation of a DFCS for active flight controls, should be thoroughly pursued, and would very likely prove to be highly beneficial for the high-angle-of-attack research program.

APPENDIX A - EQUATIONS

1.	$\Lambda = \arctan\left(\frac{b}{a}\right) = \arctan\left(\frac{k-n-l-w}{a}\right)$
2.	$\bar{x}_{cg} = \frac{W_F \bar{l}}{W_F + W_R}$
3.	$\bar{x}_{cg} = \frac{W_3 \bar{l}}{W_1 + W_2 + W_3}$
4.	$m.a.c. = \bar{c} = \frac{2}{3} c_R \left[\frac{1+\lambda+\lambda^2}{1+\lambda}\right]$
5.	$\lambda = {}^{c_T}\!/_{c_R}$
6.	$\bar{y} = \frac{b}{6}\left[\frac{1+2\lambda}{1+\lambda}\right]$
7.	$I_{cg} = \frac{P^2 a^2 (W_{MS} - W_S)}{16\pi^2 L}$
8.	$\overline{V_H} \equiv \frac{l_t S_{ht}}{\bar{c} S_w}$
9.	$\overline{V_F} \equiv \frac{l_F S_{vt}}{b S_w}$
10.	$\mu = (338.5 + 0.575 \times T) \times 10^{-9}$, where T is in ^{o}F
11.	$R_e = {}^{\rho v \bar{c}}\!/_{\mu}$
12.	$\sum \text{Rolling moments} = I_{xx}\dot{p} + qr(I_{zz} - I_{yy}) - (\dot{r} + qp)I_{xz}$ $\sum \text{Pitching moments} = I_{yy}\dot{q} + pr(I_{xx} - I_{zz}) + (p^2 - r^2)I_{xz}$ $\sum \text{Yawing moments} = I_{zz}\dot{r} + pq(I_{yy} - I_{xx}) + (qr - \dot{p})I_{xz}$

13. $$I_{xx} = \iiint_v (y^2 + z^2)\ \delta m \qquad I_{xy} = \iiint_v xy\ \delta m$$
$$I_{yy} = \iiint_v (x^2 + z^2)\ \delta m \qquad I_{xz} = \iiint_v xz\ \delta m$$
$$I_{zz} = \iiint_v (x^2 + y^2)\ \delta m \qquad I_{yz} = \iiint_v yz\ \delta m$$

14. $$\eta BHP = \frac{Tv}{550}$$

15. $$v_{max} = \frac{550\eta BHP}{T_{max}}$$

16. $$v_{max} \Rightarrow\Rightarrow\ v_{max}^4 - \frac{T_A}{.5\rho S C_{D_0}} v_{max}^2 + \frac{W^2}{(.5\rho S)^2 C_{D_0} \pi e AR} = 0$$

17. $$C_D = C_{D_0} + C_{D_i} = C_{D_0} + \frac{C_L^2}{\pi e AR}$$

18. $$D = T = .5\rho v^2 S C_D$$

19. $$T = \dot{m}_{air}(v_e - v_\infty) + (p_e - p_\infty)A_e$$

20. $$a_w = \frac{a_0}{1 + \frac{57.3 a_0}{\pi e AR}} \Rightarrow\Rightarrow \text{ or } \Rightarrow\Rightarrow a_w = \frac{a_0}{1 + \left(\frac{57.3 a_0}{\pi AR}\right)(1+\tau)}$$

21. $$v_{stall} = \sqrt{\frac{2W}{\rho S C_{L_{max}}}}$$

22. $$\partial\varepsilon/\partial\alpha = 20\left(a_w \lambda^{.3} / AR^{.725}\right)\left(3\bar{c}/l\right)^{.25}$$

23. $$h_n = h_{ac_{wb}} + V_H \frac{a_t}{a}\left(1 - \frac{\partial\varepsilon}{\partial\alpha}\right)$$

24. $$S_0 = \frac{\pi D_0^2}{4}$$

25. $$C_{D_0} = \frac{W}{.5\rho(ROD)^2 S_0}$$

26. $$ROD = \sqrt{\frac{2W}{C_{D_0} \rho S_0}}$$

APPENDIX B - EMERGENCY PARACHUTE RECOVERY SYSTEM

The original thesis student for the F/A-18 UAV project, LT Dan Lee, covered the initial parachute design in great detail [Ref. 18:pp. 34-56 and APPENDIX]. For continuity and clarification, some of his text and data will be repeated here. The reader should note the final design concept chosen for the system is similar to that of the original, but the final implementation is different.

A. DESIGN APPROACH

As stated in Reference 18, the Recovery Systems Design Guide [Ref. 37] proved an excellent reference for approaching the design needs and execution of the EPRS for the F/A-18 UAV. Many models and variations of parachute construction, applications, and specifications are contained in this guide, and some of the aerodynamic data are listed below for comparison purposes.

Chapter 2 of Reference 37 describes deployable aerodynamic decelerators (parachutes) in detail, and the particular types that are of interest here are the ordinary round parachutes, which fall into the following basic categories:

- Flat circular
- Conical, bi-conical, tri-conical, etc.
- Cross
- Ribbon type (includes the categories of flat circular and conical types)
- Annular

The flat circular and conicals are the most familiar and recognizable family

of parachutes. Primarily applications are for personnel and cargo; drone recovery and emergency parachute systems are examples. The cross and ribbon types are normally used as deceleration devices rather than for descent purposes, evidenced by their popular use by drag racers (usually the cross type) and jet aircraft with high landing speeds (usually the ribbon type).

B. DETERMINATION OF PARACHUTE REQUIREMENTS

The flat circular was the final design chosen for the aircraft. Based on a number of factors, cost being a major one, the most economical means was pursued to obtain a parachute larger than the 8.5-foot diameter parachute tested by the previous thesis student, which was found to be only marginally effective. This author, with considerable parachute jumping experience, concurred with the previous drop-testing results that the 8.5-foot flat circular parachute was inadequate (minimum descent rates were approximately 20 ft/sec), even when the apex was pulled down to increase the surface planform area and thus the drag [Ref. 18:p. 56]. (Note: the two 8.5-foot parachutes procured for this system and tests are flat circular, not the conical type as stated on page 36 of Reference 18.)

After a phone search of several government agencies involved with UAV and target drone operations, a 13-foot flat circular parachute was located at the UAV Flight Branch at the Naval Air Test Center in Patuxent River, Maryland. This brand new parachute was declared surplus and graciously donated to the Naval Postgraduate School's Aeronautics and Astronautics UAV Lab, saving approximately 300 to 500 dollars, for which NPS is quite grateful. The fabric material appears to be 1.1 oz./yd material. The suspension lines are regular braided nylon of 220-pound tensile strength.

Table B-1 is repeated in part from Reference 18. The reader should note

that the normal convention for the surface area used in the determination of C_{D_0} is the parachute's uninflated shape as spread out on a flat surface, or in other words, its flat planform area (Equation 24) [Ref. 37].

TABLE B-1
Example Parachute Types

TYPE	D_c/D_0	D_p/D_0	C_{D_0}	C_x	Oscillation
Flat Circular	1.00	.67-.70	.75-.90	1.8	10-40°
Conical	.93-.95	.70	.75-.90	1.8	10-30°
Hemispherical	.71	.66	.62.77	1.6	10-15°
Annular	1.04	.94	.95-1.0	1.4	< 6°
Cross	1.15-1.19	.66-.72	.60-.78	1.2	0-3°

The flat circular parachute is simple, inexpensive, and quite reliable by design. With the EPRS requirements being very simple, the flat circular design seemed adequate. Other types, like the conicals and the hemispherical, tend to be more expensive and offer little improvement in stability, although in larger applications they are very good for personnel systems, such as ejection seats. The annular, although quite promising in its drag coefficient, showed no real advantage beyond that, and no reliability or precedent data as a recovery parachute was available. The cross parachute has a real advantage in stability, and would likely have been the next logical step if drop testing of the current 13-foot flat circular had been deemed unsatisfactory, as stated on page 67 of Reference 18.

As in the previous parachute drop tests, a rappelling tower at nearby Fort

Ord, California was used for drop testing the 13-foot parachute. The same plywood and 4X4 inch wooden airplane mockup was employed, with a weight of 36 pounds. The drops were video taped. The tower is 41 feet tall at the upper platform level. A halfway point (20.5 feet) down the rappelling tower was noted on the video tape; the timing was started as the mockup passed that point and terminated upon impact with the ground. Five drops were made from that height. Additionally, a 30-foot high window/ledge was used for one drop, with the specific purpose to attempt to have the parachute suspension lines already stretched and the canopy nearly inflated as the wooden mockup was thrown off. This particular drop was very successful, with the canopy inflating quickly with little oscillation. However, the use of the window was difficult to execute and presented undue hazard to the parachute in the form of splinters and tears to the canopy. Pressure, temperature and wind data were recorded to obtain calculations for air density and thus to determine the coefficient of drag for the parachute. During analysis of the videotape, each drop was timed five times to build a statistical data base to allow for timing errors.

Average times and standard deviation using linear regression were calculated. Using the halfway point, the average rate of descent (ROD) was determined, which was satisfactory for the requirements of the F/A-18 UAV. Using this data, a value for the parachute's characteristic coefficient of drag (C_{D_0}) was determined from Equation 25. The reader may note that the value of C_{D_0} of 1.19 is substantially more than the typical 0.75 to 0.90 noted in Table B-1. The results were carefully recalculated several times, with the same answer. No explanation is readily available, except that perhaps the canopy material porosity is different than assumed. Nevertheless, this writer cannot argue with

both the quantitative and qualitative results of the drop tests. Having participated in the earlier drop tests, the parachute dramatically had a lower rate of descent once the canopy inflated. Results are shown in Table B-2. If the C_{D_0} of a parachute is already known, the ROD may be calculated using Equation 26.

TABLE B-2
Parachute Drop Test Data

Environmental conditions (18 April 1991) Temperature Air pressure Wind Air density (ρ), slug/ft.^{3}	 58 deg. F 14.74 psi 6 to 7 knots, steady 0.002387
Average rate of descent	13.8 ft/sec
Standard deviation -- σ	0.0445
Computed Drag Coefficient -- C_{D_0} [Equation 25]	1.19

C. EPRS INSTALLATION

Figure B-1 is a representative sketch of what the deployed parachute would look like. The parachute, lines, shock-absorbing webbing and upper risers are packed into a fiberglass tray, located within the cockpit area under the aircraft canopy, and secured by four allen screws (Figure B-2). The deployment reefing device is a diaper sewn onto the base of the skirt, and is used instead of a sleeve, which is most the common deployment device on round parachutes. The diaper saves weight and bulk, both of which became big concerns when the needs were evident to acquire a larger parachute.

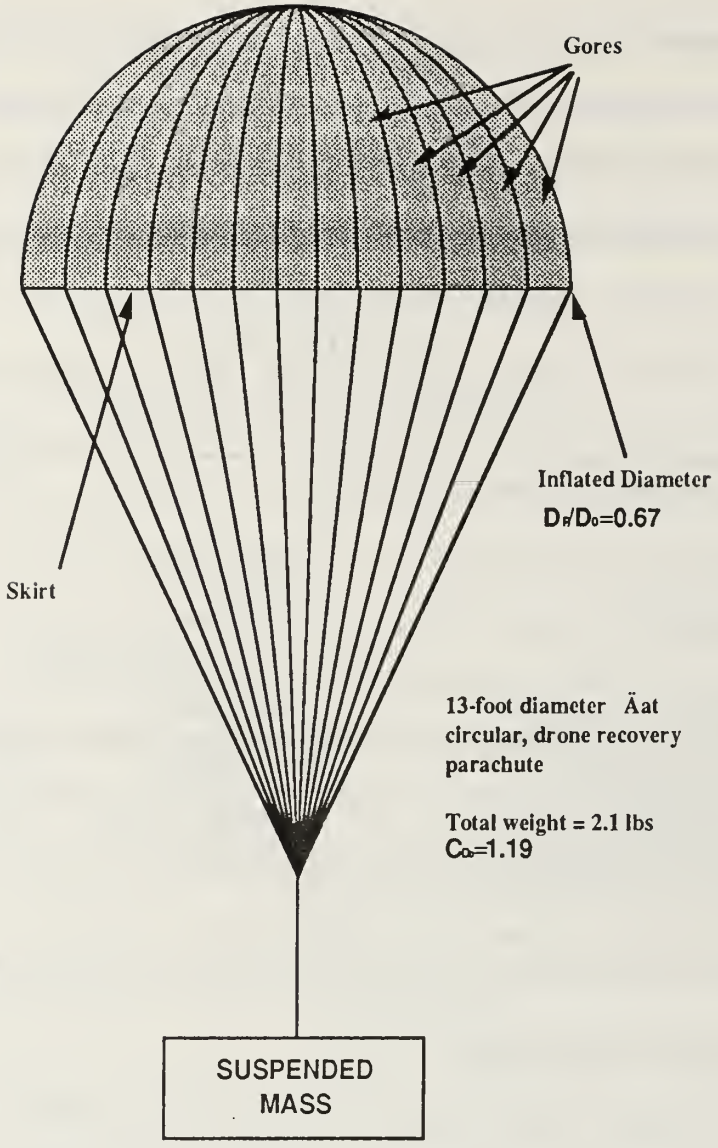

Figure B-1 Inflated profile of flat circular parachute used for the F/A-18 Emergency Parachute Release System.

The parachute is first stretched out to its full length, then "flaked" until all the gores are neatly folded upon themselves. The diaper is then wrapped around the skirt and held closed by the stowing of the suspension lines in rubber bands. This ensures that the canopy's skirt will not open and inflate during deployment

until the suspension lines are fully stretched out. The upper part of the risers are laid into the bottom of the tray, leaving enough slack for the connector ends to reach aft to the attachment points in the engine bay. The parachute is then S-folded onto itself into the tray.

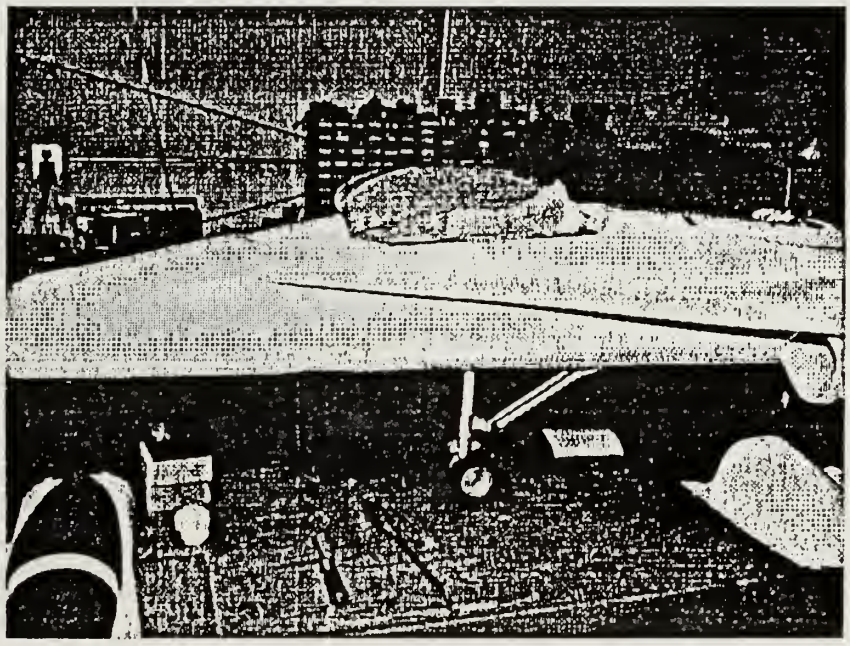

Figure B-2 Installation of parachute in the cockpit.

The pilot chute is a soft, solid-cloth type, designed for use as a pull-out pilot chute (POP) for main canopies in sport parachuting systems. It has no spring, thus something is needed to positively launch it into the airstream so it will

extract the recovery parachute. This is accomplished by attaching the pilot chute apex via hook-and-loop tape to the inside top of the aircraft's canopy. The aircraft canopy is hinged at the rear and held securely at the front by a servo actuated pin. At the very front of the canopy, a piece of very resilient foam rubber is wedged between the canopy and glareshield. Upon activation of the EPRS, the retaining pin is retracted and the foam rubber gives the front of the canopy the initial push up and away from the aircraft. Airloads are then depended upon to continue rotating the canopy upward, pulling the pilot chute with it. The rear of the canopy has only a partial hinge, and will separate from the aircraft after approximately 40° to 60° of rotation. The hook-and-loop tape was tested to separate with about three to five pounds of force, but previous testing has shown no adverse results if the canopy somehow remains attached to the parachute. The deployment system was extensively tested [Ref. 18], and the only difference between the current design and the previous testing is that the foam rubber is used now vice a spring to perform the initial separation of the canopy. Video footage of the previous testing clearly indicated that the airloads were responsible for virtually all the canopy separation once it "cracked" away from the closed position. The spring could not have possibly caused such rapid rotation away from the model's forward fuselage mockup used for the tests.

The only caveat of concern is that the EPRS will hopefully be deployed only while the model has some forward velocity. Since the parachute is not ballistically launched, such as with a mortar system or powerful spring-loaded pilot chute, it may experience some delay in deployment if the model is in some unusual attitude, such as that in a spin or tumbling flight. For this reason, the aircraft research maneuvers should be conducted at higher altitudes (at least 300

to 500 ft), and a safety observer standing by with the authority to order the UAV pilot to "put 'er in the chute". Unusual attitudes also are the reason why the airspeed transducer should be located on a wingtip or other remote location, to reduce the possibility of entanglement with the parachute in the event of deployment. Unless absolutely unavoidable, no probes or equipment of any kind should be located on the vertical tails, and such items should be located as far outboard of the aircraft centerline as possible, away from the probable deployment path of the parachute as it is extracted from the cockpit.

The parachute recovery system specifications are shown in Table B-3.

TABLE B-3
Emergency Parachute Recovery System

Parachute design	Drone-recovery type, flat circular
Diameter	13 ft.
Area -- S_0	132.7 ft.^{2}
Parachute Drag Coeff. -- C_{D_0}	1.19
Total system weight	2.1 lbs.
System activation	Manually or automatically activated servo-controlled, pin-retained, spring loaded aircraft canopy extracts pilot chute via hook and loop attachment.
D_C/D_0	1.00
l_l/D_0	1.00 (approximately)

REFERENCES

1. Bowman, John S., and others, Report SP-3070, *The Vietnam War: An Almanac*, pp. 406 and 413, Ballantine Books, 1985.

2. Murri, Daniel G., and Rao, Dhanvada M., "Exploratory Studies of Actuated Forebody Strakes for Yaw Control at High Angles of Attack", *AIAA Paper 87-2557*, Presented at the Atmospheric Flight Mechanics Conference, Monterey, California, 17-19 August 1987.

3. Ng, T.T., and Malcolm, G.N., "Aerodynamic Control Using Forebody Strakes", *AIAA Paper 90-0618,* Presented at the 29th Aerospace Sciences Meeting, Reno, Nevada, 7-10 January 1991.

4. Malcolm, Gerald N., and others, "Development of Non-Conventional Control Methods for High Angle of Attack Flight Using Vortex Manipulation", *AIAA Paper 89-2152-CP*, Presented at the 7th Applied Aerodynamics Conference, Seattle, Washington, 31 July-2 August 1989.

5. Tavella, Domingo A., Schiff, Lewis B., and Cummings, Russell M., "Pneumatic Vortical Flow Control at High Angles of Attack", *AIAA Paper 90-0098*, Presented at the 28th Aerospace Sciences Meeting, Reno, Nevada, 8-11 January 1990.

6. Telephone conversations between Mr. Richard White of NASA Langley, and the author, 12 July 1991, and previous dates.

7. Henderson, Breck W., "NASA 'Flies' F/A-18 In Ames' Largest Wind Tunnel", *Aviation Week and Space Technology*, v. 135, pp. 38-40, 29 July 1991.

8. Telephone conversation between Mr. George Makowiec of NASA Langley's Plum Tree outlying field UAV facility, and the author, 12 July 1991.

9. Fratello, David J., Croom, Mark A., Nguyen, Luat T., and Domack, Christopher S., "Use of the Updated NASA Langley Radio-Controlled Drop-Model Technique for High-Alpha Studies of the X-29A Configuration", *AIAA Paper 87-2559-CP*, Presented at the AIAA Atmospheric Flight Mechanics Conference, Monterey, California, 17-19 August 1987.

10. Telephone conversation between Mr. John Marshall of the Naval Air Test Center UAV Branch, and the author, 12 July 1991.

11. Yip, Long P., Fratello, David J., Robelen, David B., and Makowiec, George M., "Wind-Tunnel and Flight-Test Investigation of the Exdrone Remotely Piloted Vehicle Configuration", *AIAA Paper 90-1261*, Presented at the AIAA/SFTE/DGLR/SETP 5th Biannual Flight Test Conference, Ontario, California, 21-24 May 1990.

12. Yip, Long P., Robelen, David B., and Meyer, Holly. F., "Radio-Controlled Model Flight Tests of a Spin Resistant Trainer Configuration", *AIAA Paper 88-2146*, Presented at the 4th Flight Test Conference, San Diego, California, 18-20 May 1988.

13. French, K. E., "Flight Test Experience with an RPV Emergency (Parachute) Recovery System", *AIAA Paper 88-2139*, Presented at the 4th Flight Test Conference, San Diego, California, 18-20 May 1988.

14. Lovece, Joseph A., "UAV Programs Experience Growth Pains", *Armed Forces JOURNAL International,* pp. 30, 32 and 33, July 1991.

15. "Unmanned 'Toy' Played Big Role in U.S. Targeting of Iraqi Forces", *Navy Times*, v. 41, pp. 8-11, 11 March 1991.

16. Telephone conversation between Col. Larry Karch of the Pioneer UAV Systems, Joint Program Office, and the author, 16 July 1991.

17. Brunswick Corporation Defense Division, *White Paper - RATIONALE AND ADVANCED PLANNING INFORMATION FOR A POWERED-TALD*, pp. 0 and 2, April 1988.

18. Lee, Daniel M., *Development of a 1/7TH Scale Fighter UAV for Flight Research,* Master's Thesis, Naval Postgraduate School, Monterey, California, September 1990.

19. Cruise Missiles Project Office and Unmanned Aerial Vehicle Joint Project Office, *TEST AND EVALUATION MASTER PLAN (TEMP) FOR THE MEDIUM RANGE UNMANNED AERIAL VEHICLE (UAV-MR)*, pp. 1-1, 2, 3 and 4, 19 June 1991.

20. Howard, Richard M., Lyons, Daniel F., and Tanner, James C., "Research Flight Test of a Scaled Unmanned Air Vehicle", *Society of Flight Test Engineers Paper*, Presented at the 21st Annual Symposium Proceedings, Garden Grove, California, 6-10 August 1990.

21. ASSEMBLY INSTRUCTIONS and BLUEPRINTS, *F/A-18 Hornet Radio Controlled Model Kit*, Yellow Aircraft Company, Puyallup, Washington, 1990.

22. Shah, Gautam H., "Windtunnel Investigation and Tail Buffet Characteristics of Leading-Edge Extension Modifications to the F/A-18", *AIAA Paper 91-2889-CP*, Presented at the 1991 Atmospheric Flight Mechanics Conference, New Orleans, Louisiana, 12-14 August 1991.

23. Telephone conversation with Mr. Tom Cook of Jet Model Products, and the author, 9 November 1990.

24. NASA Langley Research Center, Report SP-3070, *Summary of Transformation Equations and Equations of Motion Used in Free-Flight and Wind-Tunnel Data Reduction and Analysis*, Gainer, Thomas G., and Hoffman, Sherman, pp. 84-86 and 118, 1972.

25. Department of the Navy, Naval Air Systems Command, NAVAIR A1-F18AC-NFM-000, *F/A-18A/B/C/D NATOPS Flight Manual*, 15 January 1991.

26. Facsimile receipt from Mr. Glen Weichelt of McDonnell Aircraft Company, to the author, 15 July 1991.

27. Telephone conversation with Mr. Tom Cook of Jet Model Products, and the author, 24 July 1991.

28. Hall, Stan, "Dynamic Modeling", *Sport Aviation*, v. 36, pp. 30-36, July 1987.

29. Anderson, John D., Jr., *Fundamentals of Aerodynamics*, pp. 25, 191 and 256, McGraw-Hill, Inc., 1984.

30. Nelson, Robert C., *Flight Stability and Automatic Control*, pp. 87 and 172, McGraw-Hill, Inc., 1989.

31. Parker, H. Keith, *The Design and Initial Construction of a Composite RPV for Flight Research Applications*, Master's Thesis, Naval Postgraduate School, Monterey, California, September 1988.

32. Anderson, John D., Jr., *Introduction to Flight*, pp. 216-225, McGraw-Hill, Inc., 1989.

33. Abbott, Ira H., and von Doenhoff, Albert E., *Theory of Wing Sections*, 2nd ed., pp. 562-563, Dover Publications, Inc., New York, 1959.

34. Shelton, Michael S., *Flight Test of a Merlin III Twin Turboprop Aircraft*, AE 4323 "Flight Test Engineering" Course, Flight Test Report, 20 June 1991.

35. Roberts, Sean C., *Light Aircraft Performance for Test Pilots and Flight Test Engineers*, p. 2.4, Flight Research, Inc., Flight Test Operations, Mojave, California.

36. Wilhelm, Kevin T., *Development and Testing of an Airborne Telemetry System*, Master's Thesis, Naval Postgraduate School, Monterey, California, September 1991.

37. Air Force Flight Dynamics Laboratory, AFFDL-TR-78-151, *Recovery Systems Design Guide*, Ewing, E.G., Bixby, H.W., and Knacke, T.W., December 1978.

INITIAL DISTRIBUTION LIST

No. Copies

1. Defense Technical Information Center 2
   Cameron Station
   Alexandria, VA 22304-6145

2. Library, Code 52 2
   Naval Postgraduate School
   Monterey, CA 93943-5002

3. Chairman, Code AA 1
   Department of Aeronautics and Astronautics
   Naval Postgraduate School
   Monterey, CA 93943-5000

4. Professor Richard M. Howard, Code AAHo 3
   Department of Aeronautics and Astronautics
   Naval Postgraduate School
   Monterey, CA 93943-5000

5. LCDR Michael S. Shelton 2
   3052 Damascus Trail
   Virginia Beach, VA 23456

6. Mr. Richard J. Foch 1
   Naval Research Laboratory
   Code 5712
   4555 Overlook Avenue, S.W.
   Washington, D.C. 20374

7. David Lewis 1
UAV Joint Project Office, NAVAIR
Code PDA-14UD
Washington, D.C. 20361-1014

8. Thomas S. Momiyama 2
Michael J. Harris
AIR-530T
Naval Air Systems Command
Washington, D.C. 20361-5300

9. Richard White 1
Mail Stop 355
NASA Langley Research Center
Hampton, VA 23665-5225